INTERNATIONAL JOURNAL OF
NUMERICAL ANALYSIS AND MODELING
Volume 22, Number 1, Pages 40–70

doi: 10.4208/ijnam2025-1003

A LINEARIZED, DECOUPLED AND UNCONDITIONALLY STABLE BDF2 FEM FOR THE ACTIVE FLUID MODEL

YUXING ZHANG AND BO WANG*

Abstract. In this paper, we develop a linear and decoupled fully discrete mixed finite element scheme for the active fluid model. The scheme employs an auxiliary variable to reformulate the fourth-order derivative term, an implicit-explicit treatment to deal with the nonlinear terms and the second-order pressure-projection method to split the velocity and pressure. Through rigorous theoretical analysis, the unique solvability, unconditional stability and error estimates of the numerical scheme are obtained. Then, several numerical experiments are presented to verify the efficiency and accuracy of the proposed scheme. Finally, the comparison of simulation results with laboratory results, including the motion direction of active fluid changes from disorder to order and reversal in 2D and 3D, demonstrate that the scheme can accurately capture and handle the complex dynamics of active fluid motion.

Key words. Active fluid, error estimates, auxiliary variable, BDF2, pressure-projection.

1. Introduction

The active fluid refers to a collection of particles, macro-molecules or cells that are commonly found suspended in a viscous fluid. Examples abound in the natural world, ranging from liquid-crystal-like arrangements and microbial suspensions to the coherent macro-scale dynamics exhibited by schools of fish and flocks of birds [3,7,15,17,28,42,46]. The active fluid can absorb energy from their surroundings and convert it into kinetic energy, it exhibits sought-after properties such as collective and organized motion that set it apart from classical complex fluid [25, 31]. These characteristics have attracted considerable interest from researchers in the fields of materials science, biology, medicine and other related disciplines.

For investigating the collective and organized motion of active fluid, many researchers studied active fluid in the laboratory [10, 14, 18, 23, 25, 34, 36, 38, 39, 45, 53]. Nédélec et al. [23] studied the extend and characteristics of self-organization using microtubules and molecular motors, and obtained a variety of self-organization structures. In [38], Schaller et al. investigated the phenomenon of collective motion in highly concentrated actin filaments. The obtained results demonstrate that, beyond a critical density threshold, the actin filaments undergo self-organization, forming coherent structures characterized by persistent density modulations. Guillaume et al. reported the observation of four distinct spatial instabilities within a specific cytoskeletal active gel in [35]. Their findings reveal that these instabilities are controlled by the concentrations of Adenosine triphosphate and depletion agent. However, it is difficult to culture active fluid in the laboratory, which limits the study of active fluid.

As we all know, mathematical models can help to understand the collective and organized motion of active fluid, which can capture the dynamics of active system qualitatively or quantitatively [22, 37, 40, 41, 43, 44]. Toner et al. derived a nonequilibrium continuum dynamical model based on symmetry considerations

Received by the editors on September 28, 2023 and, accepted on September 2, 2024.
2000 *Mathematics Subject Classification.* 65M12, 65M15, 65M60.
*Corresponding author.

to explore the dynamics of "flocking" behavior among living things in [40]. In [37], Simha and Ramaswamy constructed the equations of motion for small, long-wavelength disturbances in suspensions of self-propelled particles that exhibit polar and apolar ordering, utilizing symmetry principles and conservation laws. Based on the interaction and feedback between the swimming Bacillus subtilis and the fluid, Wolgemuth presented a two-phase model for the bacterial/fluid mixture [43]. But above-mentioned models ignore Pascal's law or the extremely effective suppression of density fluctuations by isotropic pressure, which is essential for the ordered state of active system. In addition, these models focus on the couplings with two or more order-parameters and typically involve a large number of parameters, making it is very difficult to compare with experimental data. Subsequently, Wensink et al. [44] derived an active fluid model based on the non-equilibrium free energy of active particle motion combined with general transport laws. The basic governing equations read as follows

$$\text{(1a)}\quad \boldsymbol{u}_t - \mu\Delta\boldsymbol{u} + \gamma\Delta^2\boldsymbol{u} + \nu(\boldsymbol{u}\cdot\nabla)\boldsymbol{u} + \alpha\boldsymbol{u} + \beta|\boldsymbol{u}|^2\boldsymbol{u} + \nabla p = \boldsymbol{f}, \quad \text{in } \Omega\times(0,T],$$

$$\text{(1b)}\quad \nabla\cdot\boldsymbol{u} = 0, \quad \text{in } \Omega\times(0,T],$$

$$\text{(1c)}\quad \boldsymbol{u}|_{t=0} = \boldsymbol{u}_0(\boldsymbol{x}), \quad \text{in } \Omega,$$

$$\text{(1d)}\quad \boldsymbol{u}|_{\partial\Omega} = \frac{\partial\boldsymbol{u}}{\partial\boldsymbol{n}}|_{\partial\Omega} = \boldsymbol{0},$$

where Ω is a smooth, bounded and connected domain in $\mathbb{R}^d$ (d=2 or 3), T is the final time and $\boldsymbol{n}$ denotes the unit outer normal vector on $\partial\Omega$. The prescribed function $\boldsymbol{u}(\boldsymbol{x},t)$, $p(\boldsymbol{x},t)$, $\boldsymbol{f}(\boldsymbol{x},t)$ and $\boldsymbol{u}_0(\boldsymbol{x})$ respectively represent the velocity, pressure, external body force and initial velocity with $\nabla\cdot\boldsymbol{u}_0 = 0$. The model parameters μ, γ and ν represent the viscosity coefficient, the generic stability coefficient and the density coefficient, which are positive. The (α,β)-terms denote a quartic Landau velocity potential, where $\beta > 0$ is positive, and α is allowed to take positive or negative values. For $\alpha > 0$, the potential is mono-stable and the fluid is damped towards a disordered state with $\boldsymbol{u} = \boldsymbol{0}$. For $\alpha < 0$, equation describes a sombrero potential with fixed points $|\boldsymbol{u}| = \sqrt{|\alpha|/\beta}$ corresponding to global polar order [7,16,44]. This paper mainly focuses on the self-organization of active fluid to the global polar order state. Due to the presence of fourth-order derivative term and strong nonlinear terms in the active fluid model, analytical solution is unattainable, necessitating the use of numerical methods for solving the system.

Now, we review some works that have been done for the active fluid model (1). Dunkel et al. in [8] showed that the model effectively captures the experimental characteristics of self-sustained active turbulence, encompassing the suppression of density fluctuations and the occurrence of continuous phase transformations. James et al. [16] numerically simulated the model using pseudo-spectral codes combined with the second-order Runge-Kutta method and found a highly ordered lattice states in an extensive turbulent transient. In [29], Reinken et al. employed the pseudo-spectral method to solve the model and demonstrated how arrays of small pillars, with minimal geometrical constraints, stabilize complex vortex lattices within a turbulent bacterial suspension. It should be noted that the above research mainly focus on numerical simulations of the active fluid model and lack the numerical analysis. Motivated by this, the primary objective of this paper is to develop a highly efficient fully discrete numerical scheme for the active fluid model and conduct a numerical analysis.

To accomplish the aforementioned aim for active fluid system, several proven methods are assembled. First, an auxiliary variable $\boldsymbol{w} = -\Delta\boldsymbol{u}$ is used to transform

the original system into an equivalent coupled nonlinear second-order equations, and the spatial domain is discretized by the mixed finite element method. The introduction of auxiliary variable improves the computational efficiency and precision of the numerical scheme. Second, we adopt the second-order pressure-projection method to solve the system, which has the ability to get second-order temporal accuracy and split the velocity and pressure [12, 32, 47, 51]. Third, the rigorous theoretical analysis of the unique solvability, unconditional stability and error estimates of the proposed scheme are given in detail. Extensive numerical experiments are then presented to validate the efficiency, stability and accuracy of the scheme, along with the simulations of various active fluid phenomena.

This paper is organized as follows. We briefly review some notations for later analysis in Section 2. We establish a linearized and decoupled fully discrete finite element scheme in Section 3, and the unique solvability and unconditional stability of the scheme are discussed in detail. In Section 4, the related error estimates are deduced rigorously. In Section 5, ample numerical experiments are carried out to testify the theoretical analysis of the error estimates and some phenomena of active fluid are simulated. In Section 6, we draw some concluding remarks.

2. Preliminaries

Now, we introduce some notations in this section. We use $\|\cdot\|_{L^s}$ to denote the usual Lebesgue space on Ω with the norm $L^s(\Omega)$. $H^r(\Omega)$ stands for the standard scalar Sobolev spaces equipped with the norm $\|\cdot\|_r$. The inner product and norm in $L^2(\Omega)$ are represented by $(\cdot,\cdot)$ and $\|\cdot\|$, respectively. Then, we define the space $L^2(0,T;H^r(\Omega))$ with the norm $\|f\|_{L^2(0,T;H^r(\Omega))} = (\int_0^T \|f\|_r^2 dt)^{\frac{1}{2}}$. Additionally, bold fonts, $\boldsymbol{L}^s(\Omega) = [L^s(\Omega)]^d$ and $\boldsymbol{H}^r(\Omega) = [H^r(\Omega)]^d$ are used for vector Sobolev spaces, and the space $L^2(0,T;\boldsymbol{H}^r(\Omega))$ is equipped with norm $\|\boldsymbol{f}\|_{L^2(0,T;\boldsymbol{H}^r(\Omega))} = (\int_0^T \sum_{i=1}^{d} \|f_i\|_r^2 dt)^{\frac{1}{2}}$.

In what follows, several function spaces are defined for the variational formulation

$$\boldsymbol{X} = \boldsymbol{H}_0^1 = \{\boldsymbol{v} \in \boldsymbol{H}^1,\ \boldsymbol{v}|_{\partial\Omega} = \boldsymbol{0}\}, \quad \boldsymbol{W} = \{\boldsymbol{\phi} \in \boldsymbol{H}^1,\ \int_\Omega \boldsymbol{\phi} d\boldsymbol{x} = 0\},$$
$$\boldsymbol{V} = \{\boldsymbol{v} \in \boldsymbol{X},\ \nabla\cdot\boldsymbol{v} = 0\}, \quad M = \{q \in L^2(\Omega),\ \int_\Omega q d\boldsymbol{x} = 0\}.$$

The function spaces $\boldsymbol{X}$ and M satisfy the inf-sup condition (see [11])

$$\|q\| \le C \sup_{\boldsymbol{v}\in\boldsymbol{X}} \frac{(q, \nabla\cdot\boldsymbol{v})}{\|\nabla\boldsymbol{v}\|},\ \forall q \in M, \tag{2}$$

where C denotes the generic positive constant that remains independent of both h and τ and may represent different values on different occasions. We define the trilinear form $b(\cdot,\cdot,\cdot)$ on $\boldsymbol{X}\times\boldsymbol{X}\times\boldsymbol{X}$ as follows

$$b(\boldsymbol{u},\boldsymbol{v},\boldsymbol{w}) = \frac{1}{2}((\boldsymbol{u}\cdot\nabla)\boldsymbol{v},\boldsymbol{w}) - \frac{1}{2}((\boldsymbol{u}\cdot\nabla)\boldsymbol{w},\boldsymbol{v}).$$

It is easy to verify that $b(\boldsymbol{u},\boldsymbol{v},\boldsymbol{w})$ satisfies (see [20, 24])

$$b(\boldsymbol{u},\boldsymbol{v},\boldsymbol{v}) = 0,\ b(\boldsymbol{u},\boldsymbol{v},\boldsymbol{w}) = -b(\boldsymbol{u},\boldsymbol{w},\boldsymbol{v}),$$
$$b(\boldsymbol{u},\boldsymbol{v},\boldsymbol{w}) \le C\|\boldsymbol{u}\|\|\nabla\boldsymbol{v}\|\|\boldsymbol{w}\|_{L^\infty},\ b(\boldsymbol{u},\boldsymbol{v},\boldsymbol{w}) \le C\|\boldsymbol{u}\|_{L^\infty}\|\nabla\boldsymbol{v}\|\|\boldsymbol{w}\|,$$
$$b(\boldsymbol{u},\boldsymbol{v},\boldsymbol{w}) \le C\|\nabla\boldsymbol{u}\|\|\nabla\boldsymbol{v}\|\|\nabla\boldsymbol{w}\|,\ b(\boldsymbol{u},\boldsymbol{v},\boldsymbol{w}) \le C\|\nabla\boldsymbol{u}\|\|\Delta\boldsymbol{v}\|\|\boldsymbol{w}\|.$$

Lemma 2.1. *(see [20, 27]) For all $\boldsymbol{\zeta}, \boldsymbol{\vartheta} \in \boldsymbol{X}$, there hold*

$$||\boldsymbol{\zeta}|^{k-2} - |\boldsymbol{\vartheta}|^{k-2}| \leq C(|\boldsymbol{\zeta}|^{k-3} + |\boldsymbol{\vartheta}|^{k-3})|\boldsymbol{\zeta} - \boldsymbol{\vartheta}|,$$
$$||\boldsymbol{\zeta}|^{k-2}\boldsymbol{\zeta} - |\boldsymbol{\vartheta}|^{k-2}\boldsymbol{\vartheta}| \leq C(|\boldsymbol{\zeta}| + |\boldsymbol{\vartheta}|)^{k-2}|\boldsymbol{\zeta} - \boldsymbol{\vartheta}|,$$
$$||\boldsymbol{\zeta}|^{k-2} - |\boldsymbol{\vartheta}|^{k-2} - (k-2)|\boldsymbol{\vartheta}|^{k-4}\boldsymbol{\vartheta} \cdot (\boldsymbol{\zeta} - \boldsymbol{\vartheta})| \leq C(|\boldsymbol{\zeta}|^{k-4} + |\boldsymbol{\vartheta}|^{k-4})|\boldsymbol{\zeta} - \boldsymbol{\vartheta}|^{k-2},$$
$$(\boldsymbol{\zeta}|\boldsymbol{\zeta}|^{k-2} - \boldsymbol{\vartheta}|\boldsymbol{\vartheta}|^{k-2}, \boldsymbol{\zeta} - \boldsymbol{\vartheta}) \geq C||\boldsymbol{\zeta} - \boldsymbol{\vartheta}||^k,$$

where C only depend on $k \geq 2$.

By employing the auxiliary variable $\boldsymbol{w} = -\Delta\boldsymbol{u}$ [26,54,57], the active fluid model (1) can be rewritten as an equivalent system

$$\boldsymbol{u}_t - \mu\Delta\boldsymbol{u} - \gamma\Delta\boldsymbol{w} + \nu(\boldsymbol{u}\cdot\nabla)\boldsymbol{u} + \alpha\boldsymbol{u} + \beta|\boldsymbol{u}|^2\boldsymbol{u} + \nabla p = \boldsymbol{f}, \quad \text{in } \Omega\times(0,T], \tag{3a}$$
$$\boldsymbol{w} = -\Delta\boldsymbol{u}, \quad \text{in } \Omega\times(0,T], \tag{3b}$$
$$\nabla\cdot\boldsymbol{u} = 0, \quad \text{in } \Omega\times(0,T], \tag{3c}$$
$$\boldsymbol{u}|_{t=0} = \boldsymbol{u}_0(\boldsymbol{x}), \quad \text{in } \Omega, \tag{3d}$$
$$\boldsymbol{u}|_{\partial\Omega} = \frac{\partial\boldsymbol{u}}{\partial\boldsymbol{n}}|_{\partial\Omega} = \boldsymbol{0}. \tag{3e}$$

Then, the weak form of the system (3) can be described in the following form: find $(\boldsymbol{u}, \boldsymbol{w}, p) \in \boldsymbol{V}\times\boldsymbol{W}\times M$ such that for all $(\boldsymbol{v}, \boldsymbol{\phi}, q) \in \boldsymbol{V}\times\boldsymbol{W}\times M$ satisfy

$$(\boldsymbol{u}_t, \boldsymbol{v}) + \mu(\nabla\boldsymbol{u}, \nabla\boldsymbol{v}) + \gamma(\nabla\boldsymbol{w}, \nabla\boldsymbol{v}) + \nu b(\boldsymbol{u}, \boldsymbol{u}, \boldsymbol{v}) + \alpha(\boldsymbol{u}, \boldsymbol{v}) + \beta(|\boldsymbol{u}|^2\boldsymbol{u}, \boldsymbol{v}) \tag{4a}$$
$$+ (\nabla p, \boldsymbol{v}) = (\boldsymbol{f}, \boldsymbol{v}), \tag{4b}$$
$$(\boldsymbol{w}, \boldsymbol{\phi}) = (\nabla\boldsymbol{u}, \nabla\boldsymbol{\phi}), \tag{4c}$$
$$(\nabla\cdot\boldsymbol{u}, q) = 0. \tag{4d}$$

The stability of the system (3) can be easily demonstrated through the standard derivation as follows.

Theorem 2.1. *Assuming $(\boldsymbol{u}, \boldsymbol{w}, p)$ is the solution of the system (4), then we have the following stability*

$$\begin{aligned} &\|\boldsymbol{u}(t)\|^2 + \int_0^t (\mu\|\nabla\boldsymbol{u}\|^2 + 2\gamma\|\boldsymbol{w}\|^2 + 2\alpha\|\boldsymbol{u}\|^2 + 2\beta\|\boldsymbol{u}\|_{L^4}^4)ds \\ &\leq \|\boldsymbol{u}_0\|^2 + C\int_0^t \|\boldsymbol{f}\|^2 ds. \end{aligned} \tag{5}$$

Proof. By taking $\boldsymbol{v} = \boldsymbol{u}$ in (4a), $\boldsymbol{\phi} = \gamma\boldsymbol{w}$ in (4c) and $q = p$ in (4d), and using $\nu b(\boldsymbol{u}, \boldsymbol{u}, \boldsymbol{u}) = 0$, we get

$$(\boldsymbol{u}_t, \boldsymbol{u}) + \mu\|\nabla\boldsymbol{u}\|^2 + \gamma(\nabla\boldsymbol{w}, \nabla\boldsymbol{u}) + \alpha\|\boldsymbol{u}\|^2 + \beta\|\boldsymbol{u}\|_{L^4}^4 = (\boldsymbol{f}, \boldsymbol{u}), \tag{6}$$

and

$$\gamma\|\boldsymbol{w}\|^2 = \gamma(\nabla\boldsymbol{w}, \nabla\boldsymbol{u}). \tag{7}$$

According to the Hölder's inequality, Young's inequality and Poincaré inequality to estimate the term to the right of (6), it is easy to get

$$(\boldsymbol{f}, \boldsymbol{u}) \leq \|\boldsymbol{f}\|\|\boldsymbol{u}\| \leq \mu\|\nabla\boldsymbol{u}\|^2 + C\|\boldsymbol{f}\|^2. \tag{8}$$

Then, combining (6), (7) with (8), we have

$$\frac{d}{dt}\|\boldsymbol{u}\|^2 + \mu\|\nabla\boldsymbol{u}\|^2 + 2\gamma\|\boldsymbol{w}\|^2 + 2\alpha\|\boldsymbol{u}\|^2 + 2\beta\|\boldsymbol{u}\|_{L^4}^4 \leq C\|\boldsymbol{f}\|^2. \tag{9}$$

Therefore, the desired result (5) follows from (9) directly, indicating that the solution is stable. □

Remark 2.1. Remarkably, by utilizing the standard Galerkin process [1, 4], the above stability can demonstrate the unique solvability of the weak solution within a certain smoothness. It is worth emphasizing that the rewritten system (3) is equivalent to the original system (1). Therefore, we only need to develop time-stepping energy-stable numerical scheme for equivalent systems (3).

3. Fully discrete schemes

In this section, we will design a novel fully-discrete mixed finite element scheme for the active fluid model (3). Before the numerical scheme, we introduce some conforming finite element spaces. Let $\mathcal{T}_h$ denote a uniformly regular partition Ω as a triangle (or tetrahedron), and the mesh-width parameter $h = \max\{d_K; K \in \mathcal{T}_h\}$, where K represents an element of the partition $\mathcal{T}_h$. For the non-negative integer $l \geq 1$, $P_l(K)$ represents a polynomial of degree l on K. The discrete function spaces $\boldsymbol{X}_h \subset \boldsymbol{X}$, $\boldsymbol{V}_h \subset \boldsymbol{V}$, $\boldsymbol{W}_h \subset \boldsymbol{W}$ and $M_h \subset M$ are constructed based on the partition $\mathcal{T}_h$, where

$$\boldsymbol{X}_h = \{\boldsymbol{v}_h \in \boldsymbol{X},\ \boldsymbol{v}_h|_K \in [P_l(K)]^d\}, \quad \boldsymbol{W}_h = \{\boldsymbol{w}_h \in \boldsymbol{W},\ \boldsymbol{w}_h|_K \in [P_l(K)]^d\},$$
$$\boldsymbol{V}_h = \{\boldsymbol{v}_h \in \boldsymbol{V} \cap \boldsymbol{X}_h,\ \nabla \cdot \boldsymbol{v}_h = 0\}, \quad M_h = \{q_h \in M,\ q_h|_K \in P_{l-1}(K)\}.$$

Moreover, we make the assumption that $\boldsymbol{X}_h$ and M_h satisfy the inf-sup condition (see [11,30])

$$\|q_h\| \leq C \sup_{\boldsymbol{v}_h \in \boldsymbol{X}_h} \frac{(\nabla \cdot \boldsymbol{v}_h, q_h)}{\|\nabla \boldsymbol{v}_h\|},\ \forall\ q_h \in M_h.$$

The following known inequality will be frequently used throughout this paper [2,48]

$$\|\boldsymbol{v}_h\|_{L^s} \leq C\|\nabla \boldsymbol{v}_h\| (2 \leq s \leq 6), \quad \|\boldsymbol{v}_h\|_{L^\infty} \leq Ch^{-\frac{d}{2}}\|\boldsymbol{v}_h\|,\ \forall\ \boldsymbol{v}_h \in \boldsymbol{X}_h.$$

To obtain the error estimates, the Ritz projections are denoted as $\mathcal{P}_h : \boldsymbol{X} \to \boldsymbol{X}_h$ and $\mathcal{R}_h : \boldsymbol{W} \to \boldsymbol{W}_h$, and the orthogonal projector represents $Q_h : M \to M_h$, which meet

$$(\nabla(\boldsymbol{v} - \mathcal{P}_h\boldsymbol{v}), \nabla \boldsymbol{w}_h) = 0,\ \forall\ \boldsymbol{v} \in \boldsymbol{X},\ \boldsymbol{w}_h \in \boldsymbol{X}_h,$$
$$(\nabla(\boldsymbol{z} - \mathcal{R}_h\boldsymbol{z}), \nabla \boldsymbol{\phi}_h) = 0,\ \forall\ \boldsymbol{z} \in \boldsymbol{W},\ \boldsymbol{\phi}_h \in \boldsymbol{W}_h,$$
$$(p - Q_h p, q_h) = 0,\ \forall\ q \in M,\ q_h \in M_h.$$

We define the discrete Laplacian Δ_h satisfies

$$(\Delta_h \boldsymbol{u}_h, \boldsymbol{v}_h) = -(\nabla \boldsymbol{u}_h, \nabla \boldsymbol{v}_h),\ \forall\ \boldsymbol{u}_h,\ \boldsymbol{v}_h \in \boldsymbol{X}_h.$$

Lemma 3.1. *Assume that Ω is a convex polygon and $\mathcal{T}_h$ is a uniformly regular partition. Let $2 \leq r \leq l$, there exists a constant $C > 0$, independent of h, such that the projections $\mathcal{P}_h$ and Q_h satisfy the following error estimates (see [9, 26, 56])*

$$\|\boldsymbol{v} - \mathcal{P}_h\boldsymbol{v}\| + h\|\nabla(\boldsymbol{v} - \mathcal{P}_h\boldsymbol{v})\| \leq Ch^{r+1}\|\boldsymbol{v}\|_{r+1},\ \boldsymbol{v} \in \boldsymbol{H}^{r+1}(\Omega) \cap \boldsymbol{X},$$
$$\|\boldsymbol{z} - \mathcal{R}_h\boldsymbol{z}\| + h\|\nabla(\boldsymbol{z} - \mathcal{R}_h\boldsymbol{z})\| \leq Ch^{r+1}\|\boldsymbol{z}\|_{r+1},\ \boldsymbol{z} \in \boldsymbol{H}^{r+1}(\Omega) \cap \boldsymbol{W},$$
$$\|q - Q_h q\| \leq Ch^r\|q\|_r,\ \forall\ q \in H^r(\Omega) \cap M.$$

Given a time step $\tau > 0$ and denoted $t_n = n\tau$ for $0 \leq n \leq N$, with the final time $T = N\tau$. To simplify the presentation, the following notation will be used throughout this paper

$$\hat{a}^{k+1} = a^{k+1} - a^k,\ \hat{a}^{*,k+1} = a^{k+1} - 2a^k + a^{k-1},\ \delta_t^* a^{k+1} = \frac{3a^{k+1} - 4a^k + a^{k-1}}{2\tau},$$
$$a^{*,k} = 2a^k - a^{k-1},\ a^{**,k+1} = a^{k+1} + 2a^k - a^{k-1}.$$

By combining the second-order backward differentiation formula (BDF2) and the pressure-projection method, we construct a linear and decoupled scheme for the system (3). Given the initial data $(\boldsymbol{u}^0, \boldsymbol{w}^0, p^0)$, having computed $(\boldsymbol{u}^{n-1}, \boldsymbol{w}^{n-1}, p^{n-1})$ and $(\boldsymbol{u}^n, \boldsymbol{w}^n, p^n)$, we compute $(\boldsymbol{u}^{n+1}, \boldsymbol{w}^{n+1}, p^{n+1})$ by the following steps [5, 19, 49, 50, 52, 55, 58, 59].

Step 1. Find $(\tilde{\boldsymbol{u}}^{n+1}, \tilde{\boldsymbol{w}}^{n+1})$ as the solution of

$$\frac{3\tilde{\boldsymbol{u}}^{n+1} - 4\boldsymbol{u}^n + \boldsymbol{u}^{n-1}}{2\tau} - \mu\Delta\tilde{\boldsymbol{u}}^{n+1} - \gamma\Delta\tilde{\boldsymbol{w}}^{n+1} + \nu(\boldsymbol{u}^{*,n}\cdot\nabla)\tilde{\boldsymbol{u}}^{n+1} + \alpha\tilde{\boldsymbol{u}}^{n+1} + \beta|\boldsymbol{u}^{*,n}|^2\tilde{\boldsymbol{u}}^{n+1} + \nabla p^n = \boldsymbol{f}^{n+1}, \tag{10a}$$

$$\tilde{\boldsymbol{w}}^{n+1} = -\Delta\tilde{\boldsymbol{u}}^{n+1}, \tag{10b}$$

$$\tilde{\boldsymbol{u}}(\boldsymbol{x}, t)|_{\partial\Omega} = 0. \tag{10c}$$

Step 2. Find $(\boldsymbol{u}^{n+1}, p^{n+1})$ as the solution of

$$\frac{3\boldsymbol{u}^{n+1} - 3\tilde{\boldsymbol{u}}^{n+1}}{2\tau} + \nabla(p^{n+1} - p^n) = 0, \tag{11a}$$

$$\nabla\cdot\boldsymbol{u}^{n+1} = 0. \tag{11b}$$

Remark 3.1. Let $\mathscr{F}$ be the projector in $\boldsymbol{H}^1$ onto the divergence-free space $\boldsymbol{V}$. We infer from (11a) that $\boldsymbol{u}^{n+1} = \mathscr{F}\tilde{\boldsymbol{u}}^{n+1}$, and the numerical scheme (10)-(11) is called projection scheme (see [33]). Each step in (10)-(11) is to solve the linear equations, hence, making the scheme highly efficient and straightforward to implement.

Remark 3.2. By taking the divergence for the equation (11a), we can obtain

$$-\Delta p^{n+1} = -\frac{3}{2\tau}\nabla\cdot\tilde{\boldsymbol{u}}^{n+1} - \Delta p^n, \tag{12}$$

associated with the Neumann boundary condition $\partial_{\boldsymbol{n}}(p^{n+1} - p^n) = 0$. Therefore, we can update $\boldsymbol{u}^{n+1}$ by

$$\boldsymbol{u}^{n+1} = \tilde{\boldsymbol{u}}^{n+1} - \frac{2\tau}{3}\nabla(p^{n+1} - p^n).$$

Next, we construct the fully discrete mixed finite element numerical scheme of the system (3). The fully discrete version of (10)-(11) reads as follows.

Step 1. Find $(\tilde{\boldsymbol{u}}_h^{n+1}, \tilde{\boldsymbol{w}}_h^{n+1}) \in \boldsymbol{X}_h \times \boldsymbol{W}_h$, such that for all $(\boldsymbol{v}_h, \boldsymbol{\phi}_h) \in \boldsymbol{X}_h \times \boldsymbol{W}_h$,

$$\begin{aligned}(\frac{3\tilde{\boldsymbol{u}}_h^{n+1} - 4\boldsymbol{u}_h^n + \boldsymbol{u}_h^{n-1}}{2\tau}, \boldsymbol{v}_h) &+ \mu(\nabla\tilde{\boldsymbol{u}}_h^{n+1}, \nabla\boldsymbol{v}_h) + \gamma(\nabla\tilde{\boldsymbol{w}}_h^{n+1}, \nabla\boldsymbol{v}_h)\\ &+ \nu b(\boldsymbol{u}_h^{*,n}, \tilde{\boldsymbol{u}}_h^{n+1}, \boldsymbol{v}_h) + \alpha(\tilde{\boldsymbol{u}}_h^{n+1}, \boldsymbol{v}_h) + \beta(|\boldsymbol{u}_h^{*,n}|^2\tilde{\boldsymbol{u}}_h^{n+1}, \boldsymbol{v}_h)\\ &+ (\nabla p_h^n, \boldsymbol{v}_h) = (\boldsymbol{f}_h^{n+1}, \boldsymbol{v}_h),\end{aligned} \tag{13a}$$

$$(\tilde{\boldsymbol{w}}_h^{n+1}, \boldsymbol{\phi}_h) = (\nabla\tilde{\boldsymbol{u}}_h^{n+1}, \nabla\boldsymbol{\phi}_h). \tag{13b}$$

Step 2. Find $p_h^{n+1} \in M_h$ as the solution of

$$(\nabla(p_h^{n+1} - p_h^n), \nabla q_h) = -\frac{3}{2\tau}(\nabla\cdot\tilde{\boldsymbol{u}}_h^{n+1}, q_h). \tag{14}$$

Step 3. Find $\boldsymbol{u}_h^{n+1} \in \boldsymbol{V}_h$ from

$$(\frac{3\boldsymbol{u}_h^{n+1} - 3\tilde{\boldsymbol{u}}_h^{n+1}}{2\tau}, \boldsymbol{v}_h) + (\nabla p_h^{n+1} - \nabla p_h^n, \boldsymbol{v}_h) = 0. \tag{15}$$

Remark 3.3. The computations of the second-order scheme (13)-(15) relies on the values of $\boldsymbol{u}_h^1$ and p_h^1. We choose $\boldsymbol{u}_h^0 = \mathcal{P}_h\boldsymbol{u}_0$ and $p_h^0 = Q_h p_0$. Then, we can compute $\boldsymbol{u}_h^1$ and p_h^1 via any first order projection method.

3.1. Unique solvability.

In this subsection, we prove the unique solvability of the scheme (13)-(15) as follows by a process similar to [6, 11].

Theorem 3.1. *There exists a unique solution* $(\tilde{\boldsymbol{u}}_h^{n+1}, \tilde{\boldsymbol{w}}_h^{n+1}) \in \boldsymbol{X}_h \times \boldsymbol{W}_h$ *to* (13) *satisfying*

$$\|\nabla \tilde{\boldsymbol{u}}_h^{n+1}\| \leq \frac{C(2\tau\|\boldsymbol{f}_h^{n+1}\| + 2\tau\|p_h^n\| + 4\|\boldsymbol{u}_h^n\| + \|\boldsymbol{u}_h^{n-1}\|)}{2\mu\tau}, \tag{16}$$

and

$$\|\tilde{\boldsymbol{w}}_h^{n+1}\| = \|\Delta \tilde{\boldsymbol{u}}_h^{n+1}\| \leq \frac{C(2\tau\|\boldsymbol{f}_h^{n+1}\| + 2\tau\|p_h^n\| + 4\|\boldsymbol{u}_h^n\| + \|\boldsymbol{u}_h^{n-1}\|)}{2\sqrt{\mu\gamma}\tau}. \tag{17}$$

Proof. We rewrite (13) as

$$\begin{aligned}
&3(\tilde{\boldsymbol{u}}_h^{n+1}, \boldsymbol{v}_h) + 2\mu\tau(\nabla \tilde{\boldsymbol{u}}_h^{n+1}, \nabla \boldsymbol{v}_h) + 2\nu\tau b(\boldsymbol{u}_h^{*,n}, \tilde{\boldsymbol{u}}_h^{n+1}, \boldsymbol{v}_h) \\
&\quad + 2\gamma\tau(\nabla \tilde{\boldsymbol{w}}_h^{n+1}, \nabla \boldsymbol{v}_h) + 2\gamma\tau(\tilde{\boldsymbol{w}}_h^{n+1}, \boldsymbol{\phi}_h) - 2\gamma\tau(\nabla \tilde{\boldsymbol{u}}_h^{n+1}, \nabla \boldsymbol{\phi}_h) \\
&\quad + 2\alpha\tau(\tilde{\boldsymbol{u}}_h^{n+1}, \boldsymbol{v}_h) + 2\beta\tau(|\boldsymbol{u}_h^{*,n}|^2 \tilde{\boldsymbol{u}}_h^{n+1}, \boldsymbol{v}_h) \\
&= 2\tau(\boldsymbol{f}_h^{n+1}, \boldsymbol{v}_h) - 2\tau(\nabla p_h^n, \boldsymbol{v}_h) + 4(\boldsymbol{u}_h^n, \boldsymbol{v}_h) - (\boldsymbol{u}_h^{n-1}, \boldsymbol{v}_h).
\end{aligned} \tag{18}$$

Taking $\boldsymbol{v}_h = \tilde{\boldsymbol{u}}_h^{n+1}$ and $\boldsymbol{\phi}_h = \tilde{\boldsymbol{w}}_h^{n+1}$ in (18), dropping some positive terms, we have

$$\begin{aligned}
&2\tau\mu\|\nabla \tilde{\boldsymbol{u}}_h^{n+1}\|^2 + 2\tau\gamma\|\tilde{\boldsymbol{w}}_h^{n+1}\|^2 \\
&\leq 2\tau(\boldsymbol{f}_h^{n+1}, \tilde{\boldsymbol{u}}_h^{n+1}) - 2\tau(\nabla p_h^n, \tilde{\boldsymbol{u}}_h^{n+1}) + (4\boldsymbol{u}_h^n, \tilde{\boldsymbol{u}}_h^{n+1}) - (\boldsymbol{u}_h^{n-1}, \tilde{\boldsymbol{u}}_h^{n+1}).
\end{aligned} \tag{19}$$

By the equation of (13b), we derive the results of (16) and (17).

Next, we denote

$$\begin{aligned}
&(\mathcal{F}(\tilde{\boldsymbol{u}}_h^{n+1}, \tilde{\boldsymbol{w}}_h^{n+1}), (\boldsymbol{v}_h, \boldsymbol{\phi}_h)) \\
&= 3(\tilde{\boldsymbol{u}}_h^{n+1}, \boldsymbol{v}_h) + 2\mu\tau(\nabla \tilde{\boldsymbol{u}}_h^{n+1}, \nabla \boldsymbol{v}_h) + 2\nu\tau b(\boldsymbol{u}_h^{*,n}, \tilde{\boldsymbol{u}}_h^{n+1}, \boldsymbol{v}_h) \\
&\quad + 2\gamma\tau(\nabla \tilde{\boldsymbol{w}}_h^{n+1}, \nabla \boldsymbol{v}_h) + 2\gamma\tau(\tilde{\boldsymbol{w}}_h^{n+1}, \boldsymbol{\phi}_h) - 2\gamma\tau(\nabla \tilde{\boldsymbol{u}}_h^{n+1}, \nabla \boldsymbol{\phi}_h) \\
&\quad + 2\alpha\tau(\tilde{\boldsymbol{u}}_h^{n+1}, \boldsymbol{v}_h) + 2\beta\tau(|\boldsymbol{u}_h^{*,n}|^2 \tilde{\boldsymbol{u}}_h^{n+1}, \boldsymbol{v}_h).
\end{aligned} \tag{20}$$

From the the Cauchy-Schwarz inequality and Poincaré inequality, we easily get

$$\begin{aligned}
&(\mathcal{F}(\tilde{\boldsymbol{u}}_h^{n+1}, \tilde{\boldsymbol{w}}_h^{n+1}), (\boldsymbol{v}_h, \boldsymbol{\phi}_h)) \\
&\leq 3\|\tilde{\boldsymbol{u}}_h^{n+1}\|\|\boldsymbol{v}_h\| + 2\mu\tau\|\nabla \tilde{\boldsymbol{u}}_h^{n+1}\|\|\nabla \boldsymbol{v}_h\| + 2C\nu\tau\|\boldsymbol{u}_h^{*,n}\|_{L^\infty}\|\nabla \tilde{\boldsymbol{u}}_h^{n+1}\|\|\nabla \boldsymbol{v}_h\| \\
&\quad + 2\gamma\tau\|\nabla \tilde{\boldsymbol{w}}_h^{n+1}\|\|\nabla \boldsymbol{v}_h\| + 2\gamma\tau\|\tilde{\boldsymbol{w}}_h^{n+1}\|\|\boldsymbol{\phi}_h\| + 2\gamma\tau\|\nabla \tilde{\boldsymbol{u}}_h^{n+1}\|\|\nabla \boldsymbol{\phi}_h\| \\
&\quad + 2\alpha\tau\|\tilde{\boldsymbol{u}}_h^{n+1}\|\|\boldsymbol{v}_h\| + 2\beta\tau\|\boldsymbol{u}_h^{*,n}\|_{L^\infty}^2\|\nabla \tilde{\boldsymbol{u}}_h^{n+1}\|\|\nabla \boldsymbol{v}_h\| \\
&\leq C(\|\nabla \tilde{\boldsymbol{u}}_h^{n+1}\| + \|\nabla \tilde{\boldsymbol{w}}_h^{n+1}\|)(\|\nabla \boldsymbol{v}_h\| + \|\nabla \boldsymbol{\phi}_h\|).
\end{aligned} \tag{21}$$

Then, taking $\boldsymbol{v}_h = \tilde{\boldsymbol{u}}_h^{n+1}$ and $\boldsymbol{\phi}_h = \tilde{\boldsymbol{w}}_h^{n+1}$, and using inverse inequality, we can obtain

$$\begin{aligned}
&(\mathcal{F}(\tilde{\boldsymbol{u}}_h^{n+1}, \tilde{\boldsymbol{w}}_h^{n+1}), (\tilde{\boldsymbol{u}}_h^{n+1}, \tilde{\boldsymbol{w}}_h^{n+1})) \\
&= 3\|\tilde{\boldsymbol{u}}_h^{n+1}\|^2 + \mu\tau\|\nabla \tilde{\boldsymbol{u}}_h^{n+1}\|^2 + \beta\tau\|\boldsymbol{u}_h^{*,n}\tilde{\boldsymbol{u}}_h^{n+1}\|^2 + \alpha\tau\|\tilde{\boldsymbol{u}}_h^{n+1}\|^2 + \gamma\tau\|\tilde{\boldsymbol{w}}_h^{n+1}\|^2 \\
&\geq \mu\tau\|\nabla \tilde{\boldsymbol{u}}_h^{n+1}\|^2 + \gamma\tau\|\tilde{\boldsymbol{w}}_h^{n+1}\|^2 \\
&\geq C_0^* \left(\|\nabla \tilde{\boldsymbol{u}}_h^{n+1}\|^2 + \|\nabla \tilde{\boldsymbol{w}}_h^{n+1}\|^2\right),
\end{aligned} \tag{22}$$

where $C_0^* = \min\{\mu\tau, \frac{C\gamma\tau}{h^2}\}$.

By applying the Lax-Milgram theorem, we can obtain that the numerical scheme (13) admits a unique solution $(\tilde{\boldsymbol{u}}_h^{n+1}, \tilde{\boldsymbol{w}}_h^{n+1})$. It is easy to prove that the numerical scheme (14)-(15) has a unique solution $\boldsymbol{u}_h^{n+1} \in \boldsymbol{V}_h$ and $p_h^{n+1} \in M_h$.

□

3.2. Stability analysis.

In this subsection, we will rigorously prove that the linear and decoupled scheme (13)-(15) is unconditionally stable as follows.

Theorem 3.2. *Suppose* $(\boldsymbol{u}_h^{n+1}, p_h^{n+1}, \tilde{\boldsymbol{u}}_h^{n+1}, \tilde{\boldsymbol{w}}_h^{n+1})$ *is the solution of the fully discrete scheme* (13)-(15)*, we have*

$$\begin{aligned} &\|\boldsymbol{u}_h^{n+1}\|^2 + \|2\boldsymbol{u}_h^{n+1} - \boldsymbol{u}_h^n\|^2 + \|\hat{\boldsymbol{u}}_h^{*,n+1}\|^2 + 4\mu\tau\|\nabla\tilde{\boldsymbol{u}}_h^{n+1}\|^2 + 4\gamma\tau\|\tilde{\boldsymbol{w}}_h^{n+1}\|^2 \\ &\quad + 4\alpha\tau\|\tilde{\boldsymbol{u}}_h^{n+1}\|^2 + \frac{4\tau^2}{3}\|\nabla p_h^{n+1}\|^2 + \frac{4\tau^2}{3}\|\nabla p_h^{n+1} - \nabla p_h^n\|^2 \\ &\le \|\boldsymbol{u}_h^n\|^2 + \|2\boldsymbol{u}_h^n - \boldsymbol{u}_h^{n-1}\|^2 + \frac{4\tau^2}{3}\|\nabla p_h^n\|^2 + \frac{2C\tau}{\mu}\|\boldsymbol{f}_h^{n+1}\|^2. \end{aligned} \tag{23}$$

Furthermore, if the external body force $\boldsymbol{f}$ *is neglected, we can get the energy dissipation law*

$$E_{tot}^{n+1} \le E_{tot}^n, \tag{24}$$

where the discrete energy is defined as $E_{tot}^n = \|\boldsymbol{u}_h^n\|^2 + \|2\boldsymbol{u}_h^n - \boldsymbol{u}_h^{n-1}\|^2 + \frac{4\tau^2}{3}\|\nabla p_h^n\|^2$.

Proof. Firstly, we recall the following identity

$$(2a, 3a - 4b + c) = a^2 - b^2 + (2a - b)^2 - (2b - c)^2 + (a - 2b + c)^2. \tag{25}$$

Taking $\boldsymbol{v}_h = 4\tau\tilde{\boldsymbol{u}}_h^{n+1}$ and $\boldsymbol{\phi}_h = 4\gamma\tau\tilde{\boldsymbol{w}}_h^{n+1}$ in (13), and summing them up, because $\nu b(\boldsymbol{u}_h^{*,n}, \tilde{\boldsymbol{u}}_h^{n+1}, \tilde{\boldsymbol{u}}_h^{n+1}) = 0$ and $\beta(|\boldsymbol{u}_h^{*,n}|^2\tilde{\boldsymbol{u}}_h^{n+1}, \tilde{\boldsymbol{u}}_h^{n+1}) \ge 0$, we obtain

$$\begin{aligned} &(3\tilde{\boldsymbol{u}}_h^{n+1} - 4\boldsymbol{u}_h^n + \boldsymbol{u}_h^{n-1}, 2\tilde{\boldsymbol{u}}_h^{n+1}) + 4\mu\tau\|\nabla\tilde{\boldsymbol{u}}_h^{n+1}\|^2 + 4\gamma\tau\|\tilde{\boldsymbol{w}}_h^{n+1}\|^2 \\ &+ 4\alpha\tau\|\tilde{\boldsymbol{u}}_h^{n+1}\|^2 + 4\tau(\nabla p_h^n, \tilde{\boldsymbol{u}}_h^{n+1}) \le 4\tau(\boldsymbol{f}_h^{n+1}, \tilde{\boldsymbol{u}}_h^{n+1}). \end{aligned} \tag{26}$$

With the help of the Hölder's inequality, Young's inequality and Poincaré inequality, the right-hand side of (26) can be estimated as follows

$$\begin{aligned} 4\tau(\boldsymbol{f}_h^{n+1}, \tilde{\boldsymbol{u}}_h^{n+1}) &\le 4\tau\|\boldsymbol{f}_h^{n+1}\|\|\tilde{\boldsymbol{u}}_h^{n+1}\| \\ &\le 2\mu\tau\|\nabla\tilde{\boldsymbol{u}}_h^{n+1}\|^2 + \frac{2C\tau}{\mu}\|\boldsymbol{f}_h^{n+1}\|^2. \end{aligned} \tag{27}$$

Choosing $\boldsymbol{v}_h = 4\tau\tilde{\boldsymbol{u}}_h^{n+1}$ in (15), we have

$$(3\boldsymbol{u}_h^{n+1} - 3\tilde{\boldsymbol{u}}_h^{n+1}, 2\tilde{\boldsymbol{u}}_h^{n+1}) + 4\tau(\nabla p_h^{n+1} - \nabla p_h^n, \tilde{\boldsymbol{u}}_h^{n+1}) = 0. \tag{28}$$

Substituting (27) into (26) and adding the resulting equations (26) and (28), we derive

$$\begin{aligned} &(3\boldsymbol{u}_h^{n+1} - 4\boldsymbol{u}_h^n + \boldsymbol{u}_h^{n-1}, 2\tilde{\boldsymbol{u}}_h^{n+1}) + 2\mu\tau\|\nabla\tilde{\boldsymbol{u}}_h^{n+1}\|^2 + 4\gamma\tau\|\tilde{\boldsymbol{w}}_h^{n+1}\|^2 \\ &+ 4\alpha\tau\|\tilde{\boldsymbol{u}}_h^{n+1}\|^2 + 4\tau(\nabla p_h^{n+1}, \tilde{\boldsymbol{u}}_h^{n+1}) \le \frac{2C\tau}{\mu}\|\boldsymbol{f}_h^{n+1}\|^2. \end{aligned} \tag{29}$$

By the equation of (11b), we get

$$(\nabla \cdot (3\boldsymbol{u}_h^{n+1} - 4\boldsymbol{u}_h^n + \boldsymbol{u}_h^{n-1}), q_h) = 0. \tag{30}$$

Taking $\boldsymbol{v}_h = \frac{4\tau}{3}(3\boldsymbol{u}_h^{n+1} - 4\boldsymbol{u}_h^n + \boldsymbol{u}_h^{n-1})$ in (15) and $q_h = p_h^{n+1} - p_h^n$ in (30), we arrive at

$$\begin{aligned}&(3\boldsymbol{u}_h^{n+1} - 4\boldsymbol{u}_h^n + \boldsymbol{u}_h^{n-1}, 2\tilde{\boldsymbol{u}}_h^{n+1} - 2\boldsymbol{u}_h^{n+1})\\ &= \frac{4\tau}{3}(3\boldsymbol{u}_h^{n+1} - 4\boldsymbol{u}_h^n + \boldsymbol{u}_h^{n-1}, \nabla(p_h^{n+1} - p_h^n)) = 0.\end{aligned} \tag{31}$$

By using (25) and (31), we obtain

$$\begin{aligned}&(3\boldsymbol{u}_h^{n+1} - 4\boldsymbol{u}_h^n + \boldsymbol{u}_h^{n-1}, 2\tilde{\boldsymbol{u}}_h^{n+1})\\ &= (3\boldsymbol{u}_h^{n+1} - 4\boldsymbol{u}_h^n + \boldsymbol{u}_h^{n-1}, 2\boldsymbol{u}_h^{n+1} + 2\tilde{\boldsymbol{u}}_h^{n+1} - 2\boldsymbol{u}_h^{n+1})\\ &= \|\boldsymbol{u}_h^{n+1}\|^2 - \|\boldsymbol{u}_h^n\|^2 + \|2\boldsymbol{u}_h^{n+1} - \boldsymbol{u}_h^n\|^2 - \|2\boldsymbol{u}_h^n - \boldsymbol{u}_h^{n-1}\|^2 + \|\hat{\boldsymbol{u}}_h^{n+1}\|^2.\end{aligned} \tag{32}$$

Then, taking $q_h = \frac{8\tau^2}{3} p_h^{n+1}$ in (14), one can easily get

$$4\tau(\nabla p_h^{n+1}, \tilde{\boldsymbol{u}}_h^{n+1}) = \frac{4\tau^2}{3}(\|\nabla p_h^{n+1}\|^2 - \|\nabla p_h^n\|^2 + \|\nabla p_h^{n+1} - \nabla p_h^n\|^2). \tag{33}$$

Substituting (32)-(33) into (29), we have

$$\begin{aligned}&\|\boldsymbol{u}_h^{n+1}\|^2 + \|2\boldsymbol{u}_h^{n+1} - \boldsymbol{u}_h^n\|^2 + \|\hat{\boldsymbol{u}}_h^{*,n+1}\|^2 + 4\mu\tau\|\nabla\tilde{\boldsymbol{u}}_h^{n+1}\|^2 + 4\gamma\tau\|\tilde{\boldsymbol{w}}_h^{n+1}\|^2\\ &\quad + 4\alpha\tau\|\tilde{\boldsymbol{u}}_h^{n+1}\|^2 + \frac{4\tau^2}{3}\|\nabla p_h^{n+1}\|^2 + \frac{4\tau^2}{3}\|\nabla p_h^{n+1} - \nabla p_h^n\|^2\\ &\le \|\boldsymbol{u}_h^n\|^2 + \|2\boldsymbol{u}_h^n - \boldsymbol{u}_h^{n-1}\|^2 + \frac{4\tau^2}{3}\|\nabla p_h^n\|^2 + \frac{2C\tau}{\mu}\|\boldsymbol{f}_h^{n+1}\|^2.\end{aligned} \tag{34}$$

If we neglect the external body force $\boldsymbol{f}$, we further get the energy dissipation law (24). □

4. Error estimates

In this section, the optimal error estimates are rigorously derived for the velocity and pressure. Throughout this paper, we assume that the solution $(\boldsymbol{u}, \boldsymbol{w}, p)$ of the equivalent system (3) exists and satisfies

$$\begin{aligned}&\|\boldsymbol{u}\|_{L^2(0,T;\boldsymbol{H}^{r+1}(\Omega))} + \|\boldsymbol{w}\|_{L^2(0,T;\boldsymbol{H}^{r+1}(\Omega))} + \|\boldsymbol{u}_t\|_{L^2(0,T;\boldsymbol{H}^{r+1}(\Omega))}\\ &\quad + \|\boldsymbol{w}_t\|_{L^2(0,T;\boldsymbol{H}^{r+1}(\Omega))} + \|\boldsymbol{u}_{tt}\|_{L^2(0,T;\boldsymbol{H}^{r+1}(\Omega))} + \|\boldsymbol{u}_{ttt}\|_{L^2(0,T;\boldsymbol{L}^2(\Omega))}\\ &\quad + \|p\|_{L^2(0,T;H^r(\Omega))} + \|p_t\|_{L^2(0,T;H^r(\Omega))} \le C.\end{aligned} \tag{35}$$

For the sake of simplicity, we adopt the usual way to decompose the errors as follows

$$\begin{aligned}&\tilde{e}_{\boldsymbol{u}}^n = \boldsymbol{u}(t_n) - \tilde{\boldsymbol{u}}_h^n = \theta_{\boldsymbol{u}}^n + \tilde{\xi}_{\boldsymbol{u}}^n, \quad \theta_{\boldsymbol{u}}^n = \boldsymbol{u}(t_n) - \mathcal{P}_h\boldsymbol{u}^n, \quad \tilde{\xi}_{\boldsymbol{u}}^n = \mathcal{P}_h\boldsymbol{u}^n - \tilde{\boldsymbol{u}}_h^n,\\ &\tilde{e}_{\boldsymbol{w}}^n = \boldsymbol{w}(t_n) - \tilde{\boldsymbol{w}}_h^n = \theta_{\boldsymbol{w}}^n + \tilde{\xi}_{\boldsymbol{w}}^n, \quad \theta_{\boldsymbol{w}}^n = \boldsymbol{w}(t_n) - \mathcal{R}_h\boldsymbol{w}^n, \quad \tilde{\xi}_{\boldsymbol{w}}^n = \mathcal{R}_h\boldsymbol{w}^n - \tilde{\boldsymbol{w}}_h^n,\\ &e_{\boldsymbol{u}}^n = \boldsymbol{u}(t_n) - \boldsymbol{u}_h^n = \theta_{\boldsymbol{u}}^n + \xi_{\boldsymbol{u}}^n, \quad \theta_{\boldsymbol{u}}^n = \boldsymbol{u}(t_n) - \mathcal{P}_h\boldsymbol{u}^n, \quad \xi_{\boldsymbol{u}}^n = \mathcal{P}_h\boldsymbol{u}^n - \boldsymbol{u}_h^n,\\ &e_{\boldsymbol{w}}^n = \boldsymbol{w}(t_n) - \boldsymbol{w}_h^n = \theta_{\boldsymbol{w}}^n + \xi_{\boldsymbol{w}}^n, \quad \theta_{\boldsymbol{w}}^n = \boldsymbol{w}(t_n) - \mathcal{R}_h\boldsymbol{w}^n, \quad \xi_{\boldsymbol{w}}^n = \mathcal{R}_h\boldsymbol{w}^n - \boldsymbol{w}_h^n,\\ &e_p = p(t_n) - p_h^n = \theta_p^n + \xi_p^n, \quad \theta_p^n = p(t_n) - Q_h p^n, \quad \xi_p^n = Q_h p^n - p_h^n.\end{aligned}$$

For $0 \le n \le N$, we take $t = t_{n+1}$ in (4) and obtain

$$\begin{aligned}&(\delta_t^*\boldsymbol{u}^{n+1}, \boldsymbol{v}_h) + \mu(\nabla\boldsymbol{u}^{n+1}, \nabla\boldsymbol{v}_h) + \gamma(\nabla\boldsymbol{w}^{n+1}, \nabla\boldsymbol{v}_h) + \nu b(\boldsymbol{u}^{n+1}, \boldsymbol{u}^{n+1}, \boldsymbol{v}_h)\\ &\quad + \alpha(\boldsymbol{u}^{n+1}, \boldsymbol{v}_h) + \beta(|\boldsymbol{u}^{n+1}|^2\boldsymbol{u}^{n+1}, \boldsymbol{v}_h) + (\nabla p^n, \boldsymbol{v}_h)\\ &= (\boldsymbol{f}^{n+1}, \boldsymbol{v}_h) + (R_{\boldsymbol{u}}^{n+1}, \boldsymbol{v}_h) - (\nabla(p^{n+1} - p^n), \boldsymbol{v}_h),\end{aligned} \tag{36a}$$

$$(\boldsymbol{w}^{n+1}, \boldsymbol{\phi}_h) = (\nabla\boldsymbol{u}^{n+1}, \nabla\boldsymbol{\phi}_h), \tag{36b}$$

$$(\nabla\cdot\boldsymbol{u}^{n+1}, q_h) = 0, \tag{36c}$$

where $R_{\boldsymbol{u}}^{n+1}$ is defined as

$$R_{\boldsymbol{u}}^{n+1} = \delta_t^* \boldsymbol{u}^{n+1} - \boldsymbol{u}_t(t_{n+1}) = \frac{3\boldsymbol{u}^{n+1} - 4\boldsymbol{u}^n + \boldsymbol{u}^{n-1}}{2\tau} - \frac{\partial \boldsymbol{u}(t_{n+1})}{\partial t}.$$

Lemma 4.1. *Under the Assumption* (35)*, the truncation errors* $R_{\boldsymbol{u}}^{n+1}$ *satisfies*

$$\max_{1\le n\le N} \|R_{\boldsymbol{u}}^{n+1}\| \le C\tau^2. \tag{37}$$

Proof. Applying the Taylor expansion, we get

$$|R_{\boldsymbol{u}}^{n+1}| = |\delta_t^* \boldsymbol{u}^{n+1} - \boldsymbol{u}_t(t_{n+1})| \le C\tau \int_{t_n}^{t_{n+1}} |\boldsymbol{u}_{ttt}(\cdot, s)| ds \le C\tau^2.$$

□

Theorem 4.1. *Let* $(\tilde{\boldsymbol{u}}_h^m, \tilde{\boldsymbol{w}}_h^m, \boldsymbol{u}_h^m, p_h^m)$ *and* $(\boldsymbol{u}(t_m), \boldsymbol{w}(t_m), p(t_m))$ *be the solutions of* (13)-(15) *and* (6)*, respectively. Under Lemma 4.1, the Assumption* (35) *and* $\tau \sim h^2$*, then for all* $0 \le m \le N$*, we have*

$$\begin{aligned} &\|e_{\boldsymbol{u}}^{m+1}\|^2 + \|e_{\boldsymbol{u}}^{*,m+1}\|^2 + \|\nabla e_{\boldsymbol{u}}^{m+1}\|^2 + \tau \sum_{n=1}^{m} \|e_p^{n+1}\|^2 \\ &\le C(\tau^4 + \max\{h^{2r-2}, h^4\}). \end{aligned} \tag{38}$$

Proof. We subtract equation (13) from equation (36) to obtain the following error equations

$$\begin{aligned} &(\frac{3\tilde{e}_{\boldsymbol{u}}^{n+1} - 4e_{\boldsymbol{u}}^n + e_{\boldsymbol{u}}^{n-1}}{2\tau}, \boldsymbol{v}_h) + \mu(\nabla \tilde{e}_{\boldsymbol{u}}^{n+1}, \nabla \boldsymbol{v}_h) + \gamma(\nabla \tilde{e}_{\boldsymbol{w}}^{n+1}, \nabla \boldsymbol{v}_h) \\ &+ \nu b(\hat{\boldsymbol{u}}^{*,n+1}, \boldsymbol{u}^{n+1}, \boldsymbol{v}_h) + \nu b(e_{\boldsymbol{u}}^{*,n}, \boldsymbol{u}^{n+1}, \boldsymbol{v}_h) + \nu b(\boldsymbol{u}_h^{*,n}, \tilde{e}_{\boldsymbol{u}}^{n+1}, \boldsymbol{v}_h) \\ &+ \alpha(\tilde{e}_{\boldsymbol{u}}^{n+1}, \boldsymbol{v}_h) + \beta(|\boldsymbol{u}_h^{*,n}|^2 \tilde{e}_{\boldsymbol{u}}^{n+1}, \boldsymbol{v}_h) + \beta((\boldsymbol{u}^{*,n} + \boldsymbol{u}_h^{*,n}) \cdot e_{\boldsymbol{u}}^{*,n} \boldsymbol{u}^{n+1}, \boldsymbol{v}_h) \\ &+ \beta((\boldsymbol{u}^{**,n+1} \cdot \hat{\boldsymbol{u}}^{*,n+1}) \boldsymbol{u}^{n+1}, \boldsymbol{v}_h) + (\nabla e_p^n, \boldsymbol{v}_h) \\ &= (R_{\boldsymbol{u}}^{n+1}, \boldsymbol{v}_h) - (\nabla(p^{n+1} - p^n), \boldsymbol{v}_h), \end{aligned} \tag{39a}$$

$$(\tilde{e}_{\boldsymbol{w}}^{n+1}, \boldsymbol{\phi}_h) = (\nabla \tilde{e}_{\boldsymbol{u}}^{n+1}, \nabla \boldsymbol{\phi}_h), \tag{39b}$$

$$(\nabla \cdot e_{\boldsymbol{u}}^{n+1}, q_h) = 0. \tag{39c}$$

From (15), we obtain

$$(\frac{3e_{\boldsymbol{u}}^{n+1} - 3\tilde{e}_{\boldsymbol{u}}^{n+1}}{2\tau}, \boldsymbol{v}_h) + (\nabla(e_p^{n+1} - e_p^n), \boldsymbol{v}_h) = (\nabla(p^{n+1} - p^n), \boldsymbol{v}_h). \tag{40}$$

In what follows, we present the analysis of the error equations (39)-(40) and then establish the error estimates given in Theorem 4.1. Firstly, we make the following induction assumption for the error functions at the previous time steps

$$\|e_{\boldsymbol{u}}^{*,n}\| \le C(\tau^2 + \max\{h^{r-1}, h^2\}), \tag{41}$$

for $n \le m$. Such an induction assumption will be recovered by the error estimate at the next time step t_{n+1}.

For $n = 1$, (41) obviously holds. The induction assumption (41) (for $n \le m$) yields

$$\|\boldsymbol{u}_h^{*,n}\|_{L^\infty} \le \|\boldsymbol{u}^{*,n}\|_{L^\infty} + \|e_{\boldsymbol{u}}^{*,n}\|_{L^\infty} \le \|\boldsymbol{u}^{*,n}\|_{L^\infty} + Ch^{-\frac{d}{2}} \|e_{\boldsymbol{u}}^{*,n}\| \le C, \tag{42}$$

for $\frac{d}{2} \le \max\{r-1, 2\}$ and $\tau \le \frac{h}{\sqrt{C}}$ with $h \le h_0$, where h_0 is a small positive constant. Then, taking $\boldsymbol{v}_h = 4\tau\tilde{\xi}_{\boldsymbol{u}}^{n+1}$ and $\boldsymbol{\phi}_h = 4\gamma\tau\tilde{\xi}_{\boldsymbol{w}}^{n+1}$ in (39) and adding them up, we have

$$
\begin{aligned}
&(3\tilde{\xi}_{\boldsymbol{u}}^{n+1} - 4\xi_{\boldsymbol{u}}^{n} + \xi_{\boldsymbol{u}}^{n-1}, 2\tilde{\xi}_{\boldsymbol{u}}^{n+1}) + 4\mu\tau\|\nabla\tilde{\xi}_{\boldsymbol{u}}^{n+1}\|^2 + 4\gamma\tau\|\tilde{\xi}_{\boldsymbol{w}}^{n+1}\|^2 + 4\alpha\tau\|\tilde{\xi}_{\boldsymbol{u}}^{n+1}\|^2 \\
&= 4\tau(R_{\boldsymbol{u}}(t_{n+1}), \tilde{\xi}_{\boldsymbol{u}}^{n+1}) - 4\tau(\nabla e_p^n, \tilde{\xi}_{\boldsymbol{u}}^{n+1}) - 2\tau(\delta_t^*\theta_{\boldsymbol{u}}^{n+1}, 2\tilde{\xi}_{\boldsymbol{u}}^{n+1}) \\
&\quad - 4\gamma\tau(\theta_{\boldsymbol{w}}^{n+1}, \tilde{\xi}_{\boldsymbol{w}}^{n+1}) - 4\alpha\tau(\theta_{\boldsymbol{u}}^{n+1}, \tilde{\xi}_{\boldsymbol{u}}^{n+1}) - 4\nu\tau b(\hat{\boldsymbol{u}}^{*,n+1}, \boldsymbol{u}^{n+1}, \tilde{\xi}_{\boldsymbol{u}}^{n+1}) \\
&\quad - 4\nu\tau b(e_{\boldsymbol{u}}^{*,n}, \boldsymbol{u}^{n+1}, \tilde{\xi}_{\boldsymbol{u}}^{n+1}) - 4\nu\tau b(\boldsymbol{u}_h^{*,n}, \tilde{e}_{\boldsymbol{u}}^{n+1}, \tilde{\xi}_{\boldsymbol{u}}^{n+1}) \\
&\quad - 4\beta\tau(|\boldsymbol{u}_h^{*,n}|^2\tilde{e}_{\boldsymbol{u}}^{n+1}, \tilde{\xi}_{\boldsymbol{u}}^{n+1}) - 4\tau(\nabla(p^{n+1} - p^n), \tilde{\xi}_{\boldsymbol{u}}^{n+1}) \\
&\quad - 4\beta\tau((\boldsymbol{u}^{*,n} + \boldsymbol{u}_h^{*,n}) \cdot e_{\boldsymbol{u}}^{*,n}\boldsymbol{u}^{n+1}, \tilde{\xi}_{\boldsymbol{u}}^{n+1}) - 4\beta\tau(\boldsymbol{u}^{**,n+1} \cdot \hat{\boldsymbol{u}}^{*,n+1}\boldsymbol{u}^{n+1}, \tilde{\xi}_{\boldsymbol{u}}^{n+1}).
\end{aligned} \tag{43}
$$

Choosing $\boldsymbol{v}_h = 4\tau\tilde{\xi}_{\boldsymbol{u}}^{n+1}$ in (40), we obtain

$$
\begin{aligned}
&(3\xi_{\boldsymbol{u}}^{n+1} - 3\tilde{\xi}_{\boldsymbol{u}}^{n+1}, 2\tilde{\xi}_{\boldsymbol{u}}^{n+1}) + 4\tau(\nabla(e_p^{n+1} - e_p^n), \tilde{\xi}_{\boldsymbol{u}}^{n+1}) \\
&= 4\tau(\nabla(p^{n+1} - p^n), \tilde{\xi}_{\boldsymbol{u}}^{n+1}).
\end{aligned} \tag{44}
$$

Adding the resulting equations (43) and (44), we derive

$$
\begin{aligned}
&(3\xi_{\boldsymbol{u}}^{n+1} - 4\xi_{\boldsymbol{u}}^{n} + \xi_{\boldsymbol{u}}^{n-1}, 2\tilde{\xi}_{\boldsymbol{u}}^{n+1}) + 4\mu\tau\|\nabla\tilde{\xi}_{\boldsymbol{u}}^{n+1}\|^2 + 4\gamma\tau\|\tilde{\xi}_{\boldsymbol{w}}^{n+1}\|^2 + 4\alpha\tau\|\tilde{\xi}_{\boldsymbol{u}}^{n+1}\|^2 \\
&= 4\tau(R_{\boldsymbol{u}}(t_{n+1}), \tilde{\xi}_{\boldsymbol{u}}^{n+1}) - 4\tau(\nabla\xi_p^{n+1}, \tilde{\xi}_{\boldsymbol{u}}^{n+1}) - 2\tau(\delta_t^*\theta_{\boldsymbol{u}}^{n+1}, 2\tilde{\xi}_{\boldsymbol{u}}^{n+1}) \\
&\quad - 4\gamma\tau(\theta_{\boldsymbol{w}}^{n+1}, \tilde{\xi}_{\boldsymbol{w}}^{n+1}) + 4\tau(\theta_p^{n+1}, \nabla\cdot\tilde{\xi}_{\boldsymbol{u}}^{n+1}) - 4\alpha\tau(\theta_{\boldsymbol{u}}^{n+1}, \tilde{\xi}_{\boldsymbol{u}}^{n+1}) \\
&\quad - 4\nu\tau b(\hat{\boldsymbol{u}}^{*,n+1}, \boldsymbol{u}^{n+1}, \tilde{\xi}_{\boldsymbol{u}}^{n+1}) - 4\nu\tau b(e_{\boldsymbol{u}}^{*,n}, \boldsymbol{u}^{n+1}, \tilde{\xi}_{\boldsymbol{u}}^{n+1}) \\
&\quad - 4\nu\tau b(\boldsymbol{u}_h^{*,n}, \tilde{e}_{\boldsymbol{u}}^{n+1}, \tilde{\xi}_{\boldsymbol{u}}^{n+1}) - 4\beta\tau(|\boldsymbol{u}_h^{*,n}|^2\tilde{e}_{\boldsymbol{u}}^{n+1}, \tilde{\xi}_{\boldsymbol{u}}^{n+1}) \\
&\quad - 4\beta\tau((\boldsymbol{u}^{*,n} + \boldsymbol{u}_h^{*,n}) \cdot e_{\boldsymbol{u}}^{*,n}\boldsymbol{u}^{n+1}, \tilde{\xi}_{\boldsymbol{u}}^{n+1}) \\
&\quad - 4\beta\tau(\boldsymbol{u}^{**,n+1} \cdot \hat{\boldsymbol{u}}^{*,n+1}\boldsymbol{u}^{n+1}, \tilde{\xi}_{\boldsymbol{u}}^{n+1}).
\end{aligned} \tag{45}
$$

Taking $\boldsymbol{v}_h = \frac{4\tau}{3}(3e_{\boldsymbol{u}}^{n+1} - 4e_{\boldsymbol{u}}^{n} + e_{\boldsymbol{u}}^{n-1})$ in (40) and from the identity of (25), we can get

$$
\begin{aligned}
&(3\xi_{\boldsymbol{u}}^{n+1} - 4\xi_{\boldsymbol{u}}^{n} + \xi_{\boldsymbol{u}}^{n-1}, 2\tilde{\xi}_{\boldsymbol{u}}^{n+1}) \\
&= (3e_{\boldsymbol{u}}^{n+1} - 4e_{\boldsymbol{u}}^{n} + e_{\boldsymbol{u}}^{n-1}, 2\tilde{\xi}_{\boldsymbol{u}}^{n+1} - 2\xi_{\boldsymbol{u}}^{n+1}) - 4\tau(\delta_t^*\theta_{\boldsymbol{u}}^{n+1}, 2\tilde{\xi}_{\boldsymbol{u}}^{n+1} - 2\xi_{\boldsymbol{u}}^{n+1}) \\
&\quad + (3\xi_{\boldsymbol{u}}^{n+1} - 4\xi_{\boldsymbol{u}}^{n} + \xi_{\boldsymbol{u}}^{n-1}, 2\xi_{\boldsymbol{u}}^{n+1}) \\
&= \|\xi_{\boldsymbol{u}}^{n+1}\|^2 - \|\xi_{\boldsymbol{u}}^{n}\|^2 + \|2\xi_{\boldsymbol{u}}^{n+1} - \xi_{\boldsymbol{u}}^{n}\|^2 - \|2\xi_{\boldsymbol{u}}^{n} - \xi_{\boldsymbol{u}}^{n-1}\|^2 + \|\hat{\xi}_{\boldsymbol{u}}^{*,n+1}\|^2 \\
&\quad - 4\tau(\delta_t^*\theta_{\boldsymbol{u}}^{n+1}, \tilde{\xi}_{\boldsymbol{u}}^{n+1} - \xi_{\boldsymbol{u}}^{n+1}).
\end{aligned} \tag{46}
$$

By the equation of (14), we have

$$
\frac{3}{2\tau}(\tilde{e}_{\boldsymbol{u}}^{n+1}, \nabla q_h) = (\nabla(e_p^{n+1} - e_p^n), \nabla q_h) - (\nabla(p^{n+1} - p^n), \nabla q_h). \tag{47}
$$

Then, taking $q_h = \frac{8\tau^2}{3}\xi_p^{n+1}$ in (47), we arrive at

$$
\begin{aligned}
&4\tau(\nabla\xi_p^{n+1}, \tilde{\xi}_{\boldsymbol{u}}^{n+1}) \\
&= \frac{4\tau^2}{3}(\|\nabla\xi_p^{n+1}\|^2 - \|\nabla\xi_p^{n}\|^2 + \|\nabla\xi_p^{n+1} - \nabla\xi_p^{n}\|^2) \\
&\quad + \frac{8\tau^2}{3}(\nabla\theta_p^{n+1} - \nabla\theta_p^{n}, \nabla\xi_p^{n+1}) - \frac{8\tau^2}{3}(\nabla p^{n+1} - \nabla p^{n}, \nabla\xi_p^{n+1}) \\
&\quad - 4\tau(\nabla\xi_p^{n+1}, \theta_{\boldsymbol{u}}^{n+1}).
\end{aligned} \tag{48}
$$

Substituting (46) and (48) into (45), we derive

$$
\begin{aligned}
&\|\xi_{\boldsymbol{u}}^{n+1}\|^2-\|\xi_{\boldsymbol{u}}^{n}\|^2+\|2\xi_{\boldsymbol{u}}^{n+1}-\xi_{\boldsymbol{u}}^{n}\|^2-\|2\xi_{\boldsymbol{u}}^{n}-\xi_{\boldsymbol{u}}^{n-1}\|^2+\|\hat{\xi}_{\boldsymbol{u}}^{*,n+1}\|^2\\
&\quad+4\mu\tau\|\nabla\tilde{\xi}_{\boldsymbol{u}}^{n+1}\|^2+4\gamma\tau\|\tilde{\xi}_{\boldsymbol{w}}^{n+1}\|^2+4\alpha\tau\|\tilde{\xi}_{\boldsymbol{u}}^{n+1}\|^2+\frac{4\tau^2}{3}(\|\nabla\xi_p^{n+1}\|^2\\
&\quad-\|\nabla\xi_p^{n}\|^2+\|\nabla\xi_p^{n+1}-\nabla\xi_p^{n}\|^2)\\
&=\sum_{i=1}^{5}I_i,
\end{aligned}
\tag{49}
$$

with

$$
\begin{aligned}
I_1&=4\tau(R_{\boldsymbol{u}}^{n+1},\tilde{\xi}_{\boldsymbol{u}}^{n+1}),\\
I_2&=-4\tau(\delta_t^*\theta_{\boldsymbol{u}}^{n+1},\xi_{\boldsymbol{u}}^{n+1})-4\gamma\tau(\theta_{\boldsymbol{w}}^{n+1},\tilde{\xi}_{\boldsymbol{w}}^{n+1})+4\tau(\theta_p^{n+1},\nabla\cdot\tilde{\xi}_{\boldsymbol{u}}^{n+1})-4\alpha\tau(\theta_{\boldsymbol{u}}^{n+1},\tilde{\xi}_{\boldsymbol{u}}^{n+1}),\\
I_3&=-4\nu\tau b(\hat{\boldsymbol{u}}^{*,n+1},\boldsymbol{u}^{n+1},\tilde{\xi}_{\boldsymbol{u}}^{n+1})-4\nu\tau b(e_{\boldsymbol{u}}^{*,n},\boldsymbol{u}^{n+1},\tilde{\xi}_{\boldsymbol{u}}^{n+1})-4\nu\tau b(\boldsymbol{u}_h^{*,n},\tilde{e}_{\boldsymbol{u}}^{n+1},\tilde{\xi}_{\boldsymbol{u}}^{n+1}),\\
I_4&=-4\beta\tau(|\boldsymbol{u}_h^{*,n}|^2\tilde{e}_{\boldsymbol{u}}^{n+1},\tilde{\xi}_{\boldsymbol{u}}^{n+1})-4\beta\tau((\boldsymbol{u}^{*,n}+\boldsymbol{u}_h^{*,n})\cdot e_{\boldsymbol{u}}^{*,n}\boldsymbol{u}^{n+1},\tilde{\xi}_{\boldsymbol{u}}^{n+1})\\
&\quad-4\beta\tau(\boldsymbol{u}^{**,n+1}\cdot\hat{\boldsymbol{u}}^{*,n+1}\boldsymbol{u}^{n+1},\tilde{\xi}_{\boldsymbol{u}}^{n+1}),\\
I_5&=\frac{8\tau^2}{3}(\nabla p^{n+1}-\nabla p^{n},\nabla\xi_p^{n+1})-\frac{8\tau^2}{3}(\nabla\theta_p^{n+1}-\nabla\theta_p^{n},\nabla\xi_p^{n+1})+4\tau(\nabla\xi_p^{n+1},\theta_{\boldsymbol{u}}^{n+1}).
\end{aligned}
$$

Now, we analyze each term on the righthand side of (49). According to Lemma 4.1, integration by parts, Hölder's inequality, Young's inequality and $\tau\sim h^2$, we find

$$
I_1\le 4\tau\|R_{\boldsymbol{u}}^{n+1}\|\|\tilde{\xi}_{\boldsymbol{u}}^{n+1}\|\le\frac{\alpha\tau}{4}\|\tilde{\xi}_{\boldsymbol{u}}^{n+1}\|^2+\frac{16\tau}{\alpha}\|R_{\boldsymbol{u}}^{n+1}\|^2\le\frac{\alpha\tau}{4}\|\tilde{\xi}_{\boldsymbol{u}}^{n+1}\|^2+C\tau^5,
\tag{50}
$$

$$
\begin{aligned}
I_2&\le 4\tau\big(\|\delta_t^*\theta_{\boldsymbol{u}}^{n+1}\|\|\xi_{\boldsymbol{u}}^{n+1}\|+\gamma\|\theta_{\boldsymbol{w}}^{n+1}\|\|\tilde{\xi}_{\boldsymbol{w}}^{n+1}\|+\|\theta_p^{n+1}\|\|\nabla\tilde{\xi}_{\boldsymbol{u}}^{n+1}\|\\
&\quad+\alpha\|\theta_{\boldsymbol{u}}^{n+1}\|\|\tilde{\xi}_{\boldsymbol{u}}^{n+1}\|\big)\\
&\le\tau\|\xi_{\boldsymbol{u}}^{n+1}\|^2+\gamma\tau\|\tilde{\xi}_{\boldsymbol{w}}^{n+1}\|^2+\frac{\alpha\tau}{4}\|\tilde{\xi}_{\boldsymbol{u}}^{n+1}\|^2+\frac{\mu\tau}{3}\|\nabla\tilde{\xi}_{\boldsymbol{u}}^{n+1}\|^2+8\gamma\tau\|\theta_{\boldsymbol{w}}^{n+1}\|^2\\
&\quad+4\tau\|\delta_t^*\theta_{\boldsymbol{u}}^{n+1}\|^2+16\alpha\tau\|\theta_{\boldsymbol{u}}^{n+1}\|^2+\frac{3\tau}{4\mu}\|\theta_p^{n+1}\|^2\\
&\le\tau\|\xi_{\boldsymbol{u}}^{n+1}\|^2+\gamma\tau\|\tilde{\xi}_{\boldsymbol{w}}^{n+1}\|^2+\frac{\alpha\tau}{4}\|\tilde{\xi}_{\boldsymbol{u}}^{n+1}\|^2+\frac{\mu\tau}{3}\|\nabla\tilde{\xi}_{\boldsymbol{u}}^{n+1}\|^2+C\tau h^{2r},
\end{aligned}
\tag{51}
$$

$$
\begin{aligned}
I_3&\le 4C\nu\tau\|\nabla\tilde{\xi}_{\boldsymbol{u}}^{n+1}\|\big(\|\Delta\boldsymbol{u}^{n+1}\|(\|\hat{\boldsymbol{u}}^{*,n+1}\|+\|\theta_{\boldsymbol{u}}^{n}\|+\|\xi_{\boldsymbol{u}}^{n}\|+\|\theta_{\boldsymbol{u}}^{n-1}\|\\
&\quad+\|\xi_{\boldsymbol{u}}^{n-1}\|)+\|\boldsymbol{u}_h^{*,n}\|_{L^\infty}\|\nabla\theta_{\boldsymbol{u}}^{n+1}\|\big)\\
&\le\frac{\mu\tau}{3}\|\nabla\tilde{\xi}_{\boldsymbol{u}}^{n+1}\|^2+\frac{12C\nu^2\tau}{\mu}\|\Delta\boldsymbol{u}^{n+1}\|^2(\|\xi_{\boldsymbol{u}}^{n}\|^2+\|\xi_{\boldsymbol{u}}^{n-1}\|^2+\|\theta_{\boldsymbol{u}}^{n}\|^2\\
&\quad+\|\theta_{\boldsymbol{u}}^{n-1}\|^2)+\frac{12C\nu^2\tau}{\mu}\|\Delta\boldsymbol{u}^{n+1}\|^2\|\hat{\boldsymbol{u}}^{*,n+1}\|^2\\
&\quad+\frac{12C\nu^2\tau}{\mu}\|\boldsymbol{u}_h^{*,n}\|_{L^\infty}^2\|\nabla\theta_{\boldsymbol{u}}^{n+1}\|^2\\
&\le\frac{\mu\tau}{3}\|\nabla\tilde{\xi}_{\boldsymbol{u}}^{n+1}\|^2+C\tau(\|\xi_{\boldsymbol{u}}^{n}\|^2+\|\xi_{\boldsymbol{u}}^{n-1}\|^2)+C\tau h^{2r}+C\tau^5,
\end{aligned}
\tag{52}
$$

$$
\begin{aligned}
I_4&\le 4\beta\tau\|\nabla\tilde{\xi}_{\boldsymbol{u}}^{n+1}\|\big(\|\boldsymbol{u}_h^{*,n}\|_{L^\infty}^2\|\nabla\theta_{\boldsymbol{u}}^{n+1}\|+\|\Delta\boldsymbol{u}^{n+1}\|\|\nabla\boldsymbol{u}^{*,n+1}\|\|\boldsymbol{u}^{**,n+1}\|\\
&\quad+\|\Delta\boldsymbol{u}^{n+1}\|(\|\nabla\boldsymbol{u}^{*,n}\|+\|\boldsymbol{u}_h^{*,n}\|_{L^\infty})(\|\theta_{\boldsymbol{u}}^{n}\|+\|\xi_{\boldsymbol{u}}^{n}\|+\|\theta_{\boldsymbol{u}}^{n-1}\|+\|\xi_{\boldsymbol{u}}^{n-1}\|)\big)\\
&\le\frac{\mu\tau}{3}\|\nabla\tilde{\xi}_{\boldsymbol{u}}^{n+1}\|^2+\frac{12C\beta^2\tau}{\mu}\big(\|\boldsymbol{u}_h^{*,n}\|_{L^\infty}^4\|\nabla\theta_{\boldsymbol{u}}^{n+1}\|^2
\end{aligned}
\tag{53}
$$

$$
\begin{aligned}
&+\|\Delta \boldsymbol{u}^{n+1}\|^2\|\nabla \boldsymbol{u}^{*,n+1}\|^2\|\boldsymbol{u}^{**,n+1}\|^2+\|\Delta \boldsymbol{u}^{n+1}\|^2(\|\nabla \boldsymbol{u}^{*,n}\|^2\\
&+\|\boldsymbol{u}_h^{*,n}\|_{L^\infty}^2)(\|\theta_{\boldsymbol{u}}^n\|^2+\|\xi_{\boldsymbol{u}}^n\|^2+\|\theta_{\boldsymbol{u}}^{n-1}\|^2+\|\xi_{\boldsymbol{u}}^{n-1}\|^2))\\
&\le \frac{\mu\tau}{3}\|\nabla\tilde{\xi}_{\boldsymbol{u}}^{n+1}\|^2+C\tau(\|\xi_{\boldsymbol{u}}^n\|^2+\|\xi_{\boldsymbol{u}}^{n-1}\|^2)+C\tau h^{2r}+C\tau^5,
\end{aligned}
$$

$$
\begin{aligned}
I_5 &\le \frac{8\tau^2}{3}\int_{t_n}^{t_{n+1}}(\|\nabla p_t\|+\|\nabla\theta_{pt}\|)ds\|\nabla\xi_p^{n+1}\|+4\tau h^{r+1}\|\nabla\xi_p^{n+1}\|\\
&\le \tau^3\|\nabla\xi_p^{n+1}\|^2+C\tau^2\int_{t_n}^{t_{n+1}}\|\nabla p_t\|^2ds+C\tau^{-1}h^{2r+2}\\
&\le \tau^3\|\nabla\xi_p^{n+1}\|^2+C\tau(h^4+h^{2r-2}).
\end{aligned}
\tag{54}
$$

Substituting (50)-(54) into (49) and summing it over n from 1 to m, we obtain

$$
\begin{aligned}
&\|\xi_{\boldsymbol{u}}^{m+1}\|^2+\|2\xi_{\boldsymbol{u}}^{m+1}-\xi_{\boldsymbol{u}}^m\|^2+\frac{4\tau^2}{3}\|\nabla\xi_p^{m+1}\|^2+\sum_{n=1}^m\|\hat{\xi}_{\boldsymbol{u}}^{*,n+1}\|^2\\
&+3\mu\tau\sum_{n=1}^m\|\nabla\tilde{\xi}_{\boldsymbol{u}}^{n+1}\|^2+3\gamma\tau\sum_{n=1}^m\|\tilde{\xi}_{\boldsymbol{w}}^{n+1}\|^2+3\alpha\tau\sum_{n=1}^m\|\tilde{\xi}_{\boldsymbol{u}}^{n+1}\|^2\\
&+\frac{4\tau^2}{3}\sum_{n=1}^m\|\nabla\xi_p^{n+1}-\nabla\xi_p^n\|^2\\
&\le C\tau\sum_{n=1}^m\left(\tau^4+h^{2r-2}+h^4+\|\xi_{\boldsymbol{u}}^{n+1}\|^2+\|\xi_{\boldsymbol{u}}^n\|^2+\|\xi_{\boldsymbol{u}}^{n-1}\|^2+\tau^2\|\nabla\xi_p^{n+1}\|^2\right).
\end{aligned}
\tag{55}
$$

Employing the discrete Gronwall's inequality, it is easy to get

$$
\begin{aligned}
&\|\xi_{\boldsymbol{u}}^{m+1}\|^2+\|2\xi_{\boldsymbol{u}}^{m+1}-\xi_{\boldsymbol{u}}^m\|^2+\frac{4\tau^2}{3}\|\nabla\xi_p^{m+1}\|^2+\sum_{n=1}^m\|\hat{\xi}_{\boldsymbol{u}}^{*,n+1}\|^2\\
&+3\mu\tau\sum_{n=1}^m\|\nabla\tilde{\xi}_{\boldsymbol{u}}^{n+1}\|^2+3\gamma\tau\sum_{n=1}^m\|\tilde{\xi}_{\boldsymbol{w}}^{n+1}\|^2+3\alpha\tau\sum_{n=1}^m\|\tilde{\xi}_{\boldsymbol{u}}^{n+1}\|^2\\
&+\frac{4\tau^2}{3}\sum_{n=1}^m\|\nabla\xi_p^{n+1}-\nabla\xi_p^n\|^2\\
&\le C(\tau^4+\max\{h^{2r-2},h^4\}).
\end{aligned}
\tag{56}
$$

The above estimate implies that the induction assumption (41) could be recovered at $n=m+1$. Thus the mathematical induction is closed.

In what follows, we add the equations (39) and (40) and obtain

$$
\begin{aligned}
&(\frac{3e_{\boldsymbol{u}}^{n+1}-4e_{\boldsymbol{u}}^n+e_{\boldsymbol{u}}^{n-1}}{2\tau},\boldsymbol{v}_h)+\mu(\nabla\tilde{e}_{\boldsymbol{u}}^{n+1},\nabla\boldsymbol{v}_h)+\gamma(\nabla\tilde{e}_{\boldsymbol{w}}^{n+1},\nabla\boldsymbol{v}_h)\\
&\quad+\nu b(\hat{\boldsymbol{u}}^{*,n+1},\boldsymbol{u}^{n+1},\boldsymbol{v}_h)+\nu b(e_{\boldsymbol{u}}^{*,n},\boldsymbol{u}^{n+1},\boldsymbol{v}_h)+\nu b(\boldsymbol{u}_h^{*,n},\tilde{e}_{\boldsymbol{u}}^{n+1},\boldsymbol{v}_h)\\
&\quad+\beta(|\boldsymbol{u}_h^{*,n}|^2\tilde{e}_{\boldsymbol{u}}^{n+1},\boldsymbol{v}_h)+\beta((\boldsymbol{u}^{*,n}+\boldsymbol{u}_h^{*,n})\cdot e_{\boldsymbol{u}}^{*,n}\boldsymbol{u}^{n+1},\boldsymbol{v}_h)\\
&\quad+\beta((\boldsymbol{u}^{**,n+1}\cdot\hat{\boldsymbol{u}}^{*,n+1})\boldsymbol{u}^{n+1},\boldsymbol{v}_h)+(\nabla e_p^{n+1},\boldsymbol{v}_h)+\alpha(\tilde{e}_{\boldsymbol{u}}^{n+1},\boldsymbol{v}_h)\\
&=(R_{\boldsymbol{u}}^{n+1},\boldsymbol{v}_h),
\end{aligned}
\tag{57a}
$$

$$
(\tilde{e}_{\boldsymbol{w}}^{n+1},\boldsymbol{\phi}_h)=(\nabla\tilde{e}_{\boldsymbol{u}}^{n+1},\nabla\boldsymbol{\phi}_h),
\tag{57b}
$$

$$
(\nabla\cdot e_{\boldsymbol{u}}^{n+1},q_h)=0.
\tag{57c}
$$

Then, taking $\boldsymbol{v}_h = 4\tau\delta_t^*\xi_{\boldsymbol{u}}^{n+1}$ in (57a), one has

$$
\begin{aligned}
&4\tau\|\delta_t^*\xi_{\boldsymbol{u}}^{n+1}\|^2 + 4\mu\tau(\nabla\tilde{\xi}_{\boldsymbol{u}}^{n+1}, \nabla\delta_t^*\xi_{\boldsymbol{u}}^{n+1}) + 4\gamma\tau(\nabla\tilde{\xi}_{\boldsymbol{w}}^{n+1}, \nabla\delta_t^*\xi_{\boldsymbol{u}}^{n+1})\\
&= 4\tau(R_{\boldsymbol{u}}(t_{n+1}), \delta_t^*\xi_{\boldsymbol{u}}^{n+1}) - 4\tau(\delta_t^*\theta_{\boldsymbol{u}}^{n+1}, \delta_t^*\xi_{\boldsymbol{u}}^{n+1}) - 4\alpha\tau(\theta_{\boldsymbol{u}}^{n+1}, \delta_t^*\xi_{\boldsymbol{u}}^{n+1})\\
&\quad - 4\alpha\tau(\tilde{\xi}_{\boldsymbol{u}}^{n+1}, \delta_t^*\xi_{\boldsymbol{u}}^{n+1}) + 4\tau(\nabla e_p^{n+1}, \delta_t^*\theta_{\boldsymbol{u}}^{n+1})\\
&\quad - 4\nu\tau b(\hat{\boldsymbol{u}}^*(t_{n+1}), \boldsymbol{u}(t_{n+1}), \delta_t^*\xi_{\boldsymbol{u}}^{n+1}) - 4\nu\tau b(e_{\boldsymbol{u}}^{*,n}, \boldsymbol{u}(t_{n+1}), \delta_t^*\xi_{\boldsymbol{u}}^{n+1})\\
&\quad - 4\nu\tau b(\boldsymbol{u}_h^{*,n}, \tilde{e}_{\boldsymbol{u}}^{n+1}, \delta_t^*\xi_{\boldsymbol{u}}^{n+1}) - 4\beta\tau((\boldsymbol{u}^*(t_n) + \boldsymbol{u}_h^{*,n})\cdot e_{\boldsymbol{u}}^{*,n}\boldsymbol{u}(t_{n+1}), \delta_t^*\xi_{\boldsymbol{u}}^{n+1})\\
&\quad - 4\beta\tau(|\boldsymbol{u}_h^{*,n}|^2\tilde{e}_{\boldsymbol{u}}^{n+1}, \delta_t^*\xi_{\boldsymbol{u}}^{n+1}) - 4\beta\tau(\boldsymbol{u}^{**}(t_{n+1})\cdot\hat{\boldsymbol{u}}^*(t_{n+1})\boldsymbol{u}(t_{n+1}), \delta_t^*\xi_{\boldsymbol{u}}^{n+1}).
\end{aligned}
\tag{58}
$$

By the equation (36b), (39b) and (57c), we arrive at

$$(e_{\boldsymbol{w}}^{n+1}, \boldsymbol{\phi}_h) = (\nabla e_{\boldsymbol{u}}^{n+1}, \nabla\boldsymbol{\phi}_h), \tag{59a}$$

$$(\tilde{\xi}_{\boldsymbol{w}}^{n+1} - \xi_{\boldsymbol{w}}^{n+1}, \boldsymbol{\phi}_h) = (\nabla\tilde{\xi}_{\boldsymbol{u}}^{n+1} - \nabla\xi_{\boldsymbol{u}}^{n+1}, \nabla\boldsymbol{\phi}_h), \tag{59b}$$

$$(\delta_t^*\theta_{\boldsymbol{w}}^{n+1}, \boldsymbol{\phi}_h) + (\delta_t^*\xi_{\boldsymbol{w}}^{n+1}, \boldsymbol{\phi}_h) = (\nabla\delta_t^*\xi_{\boldsymbol{u}}^{n+1}, \nabla\boldsymbol{\phi}_h), \tag{59c}$$

$$(\nabla\cdot\delta_t^* e_{\boldsymbol{u}}^{n+1}, q_h) = 0. \tag{59d}$$

Choosing $q_h = 4\mu\tau\Delta(p_h^{n+1} - p_h^n)$ in (59d), we derive

$$
\begin{aligned}
&4\mu\tau(\nabla\delta_t^*\xi_{\boldsymbol{u}}^{n+1}, \nabla\tilde{\xi}_{\boldsymbol{u}}^{n+1})\\
&= 4\mu\tau(\nabla\delta_t^*\xi_{\boldsymbol{u}}^{n+1}, \nabla\xi_{\boldsymbol{u}}^{n+1}) + 4\mu\tau(\nabla\delta_t^*\xi_{\boldsymbol{u}}^{n+1}, \nabla(\tilde{\xi}_{\boldsymbol{u}}^{n+1} - \xi_{\boldsymbol{u}}^{n+1}))\\
&= 4\mu\tau(\nabla\xi_{\boldsymbol{u}}^{n+1}, \nabla\delta_t^*\xi_{\boldsymbol{u}}^{n+1}) - 4\mu\tau(\nabla\cdot\delta_t^* e_{\boldsymbol{u}}^{n+1}, \Delta(p_h^{n+1} - p_h^{n+1}))\\
&= \mu(\|\nabla\xi_{\boldsymbol{u}}^{n+1}\|^2 - \|\nabla\xi_{\boldsymbol{u}}^n\|^2 + \|2\nabla\xi_{\boldsymbol{u}}^{n+1} - \nabla\xi_{\boldsymbol{u}}^n\|^2\\
&\quad - \|2\nabla\xi_{\boldsymbol{u}}^n - \nabla\xi_{\boldsymbol{u}}^{n-1}\|^2 + \|\nabla\hat{\xi}_{\boldsymbol{u}}^{*,n+1}\|^2).
\end{aligned}
\tag{60}
$$

Then, we taking $\boldsymbol{\phi}_h = 4\gamma\tau\tilde{\xi}_{\boldsymbol{w}}^{n+1}$ in (59c) and $q_h = 4\gamma\tau\Delta^2(p_h^{n+1} - p_h^n)$ in (59d), we have

$$
\begin{aligned}
&4\gamma\tau(\nabla\delta_t^*\xi_{\boldsymbol{u}}^{n+1}, \nabla\tilde{\xi}_{\boldsymbol{w}}^{n+1})\\
&= 4\gamma\tau(\delta_t^*\theta_{\boldsymbol{w}}^{n+1}, \tilde{\xi}_{\boldsymbol{w}}^{n+1}) + 4\gamma\tau(\delta_t^*\xi_{\boldsymbol{w}}^{n+1}, \xi_{\boldsymbol{w}}^{n+1}) + 4\gamma\tau(\delta_t^*\xi_{\boldsymbol{w}}^{n+1}, \tilde{\xi}_{\boldsymbol{w}}^{n+1} - \xi_{\boldsymbol{w}}^{n+1})\\
&= \gamma(\|\xi_{\boldsymbol{w}}^{n+1}\|^2 - \|\xi_{\boldsymbol{w}}^n\|^2 + \|2\xi_{\boldsymbol{w}}^{n+1} - \xi_{\boldsymbol{w}}^n\|^2 - \|2\xi_{\boldsymbol{w}}^n - \xi_{\boldsymbol{w}}^{n-1}\|^2 + \|\hat{\xi}_{\boldsymbol{w}}^{*,n+1}\|^2)\\
&\quad + 4\gamma\tau(\delta_t^*\theta_{\boldsymbol{w}}^{n+1}, \xi_{\boldsymbol{w}}^{n+1}).
\end{aligned}
\tag{61}
$$

Substituting (60) and (61) into (58), we obtain

$$
\begin{aligned}
&4\tau\|\delta_t^*\xi_{\boldsymbol{u}}^{n+1}\|^2 + \mu(\|\nabla\xi_{\boldsymbol{u}}^{n+1}\|^2 - \|\nabla\xi_{\boldsymbol{u}}^n\|^2 + \|\nabla\hat{\xi}_{\boldsymbol{u}}^{*,n+1}\|^2 + \|2\nabla\xi_{\boldsymbol{u}}^{n+1} - \nabla\xi_{\boldsymbol{u}}^n\|^2\\
&- \|2\nabla\xi_{\boldsymbol{u}}^n - \nabla\xi_{\boldsymbol{u}}^{n-1}\|^2) + \gamma(\|\xi_{\boldsymbol{w}}^{n+1}\|^2 - \|\xi_{\boldsymbol{w}}^n\|^2 + \|\hat{\xi}_{\boldsymbol{w}}^{*,n+1}\|^2 + \|2\xi_{\boldsymbol{w}}^{n+1} - \xi_{\boldsymbol{w}}^n\|^2\\
&- \|2\xi_{\boldsymbol{w}}^n - \xi_{\boldsymbol{w}}^{n-1}\|^2) = \sum_{i=1}^4 S_i,
\end{aligned}
\tag{62}
$$

with

$$
\begin{aligned}
S_1 &= 4\tau(R_{\boldsymbol{u}}(t_{n+1}), \delta_t^*\xi_{\boldsymbol{u}}^{n+1}),\\
S_2 &= -4\tau(\delta_t^*\theta_{\boldsymbol{u}}^{n+1}, \delta_t^*\xi_{\boldsymbol{u}}^{n+1}) - 4\alpha\tau(\theta_{\boldsymbol{u}}^{n+1}, \delta_t^*\xi_{\boldsymbol{u}}^{n+1}) - 4\alpha\tau(\tilde{\xi}_{\boldsymbol{u}}^{n+1}, \delta_t^*\xi_{\boldsymbol{u}}^{n+1})\\
&\quad + 4\tau(\nabla e_p^{n+1}, \delta_t^*\theta_{\boldsymbol{u}}^{n+1}) - 4\gamma\tau(\delta_t^*\theta_{\boldsymbol{w}}^{n+1}, \xi_{\boldsymbol{w}}^{n+1}),\\
S_3 &= -4\nu\tau b(\hat{\boldsymbol{u}}^*(t_{n+1}), \boldsymbol{u}(t_{n+1}), \delta_t^*\xi_{\boldsymbol{u}}^{n+1}) - 4\nu\tau b(e_{\boldsymbol{u}}^{*,n}, \boldsymbol{u}(t_{n+1}), \delta_t^*\xi_{\boldsymbol{u}}^{n+1})\\
&\quad - 4\nu\tau b(\boldsymbol{u}_h^{*,n}, \tilde{e}_{\boldsymbol{u}}^{n+1}, \delta_t^*\xi_{\boldsymbol{u}}^{n+1}),\\
S_4 &= -4\beta\tau(|\boldsymbol{u}_h^{*,n}|^2\tilde{e}_{\boldsymbol{u}}^{n+1}, \delta_t^*\xi_{\boldsymbol{u}}^{n+1}) - 4\beta\tau((\boldsymbol{u}^*(t_n) + \boldsymbol{u}_h^{*,n})\cdot e_{\boldsymbol{u}}^{*,n}\boldsymbol{u}(t_{n+1}), \delta_t^*\xi_{\boldsymbol{u}}^{n+1})
\end{aligned}
$$

$$- 4\beta\tau(\boldsymbol{u}^{**}(t_{n+1})\cdot\hat{\boldsymbol{u}}^{*}(t_{n+1})\boldsymbol{u}(t_{n+1}),\delta_t^*\xi_{\boldsymbol{u}}^{n+1}).$$

Recalling the Lemma 4.1, $\tau\sim h^2$, integration by parts, Hölder's inequality and Young's inequality again, the estimates for each term on the righthand side of (62) are obtained below

$$S_1 \le 4\tau\|R_{\boldsymbol{u}}(t_{n+1})\|\|\delta_t^*\xi_{\boldsymbol{u}}^{n+1}\| \le \frac{\tau}{2}\|\delta_t^*\xi_{\boldsymbol{u}}^{n+1}\|^2 + C\tau^5, \tag{63}$$

$$\begin{aligned} S_2 &\le 4\tau(\|\delta_t^*\theta_{\boldsymbol{u}}^{n+1}\|\|\delta_t^*\xi_{\boldsymbol{u}}^{n+1}\| + \alpha\|\theta_{\boldsymbol{u}}^{n+1}\|\|\delta_t^*\xi_{\boldsymbol{u}}^{n+1}\| + \alpha\|\tilde{\xi}_{\boldsymbol{u}}^{n+1}\|\|\delta_t^*\xi_{\boldsymbol{u}}^{n+1}\| \\ &\quad + \gamma\|\delta_t^*\theta_{\boldsymbol{w}}^{n+1}\|\|\xi_{\boldsymbol{w}}^{n+1}\| + \|\nabla\theta_p^{n+1}\|\|\delta_t^*\theta_{\boldsymbol{u}}^{n+1}\| + \|\nabla\xi_p^{n+1}\|\|\delta_t^*\theta_{\boldsymbol{u}}^{n+1}\|) \\ &\le \frac{\tau}{2}\|\delta_t^*\xi_{\boldsymbol{u}}^{n+1}\|^2 + \tau^3\|\nabla\xi_p^{n+1}\|^2 + 12\tau(\|\delta_t^*\theta_{\boldsymbol{u}}^{n+1}\|^2 + \alpha\|\theta_{\boldsymbol{u}}^{n+1}\|^2 + \alpha\|\tilde{\xi}_{\boldsymbol{u}}^{n+1}\|^2) \\ &\quad + \gamma\tau\|\xi_{\boldsymbol{w}}^{n+1}\|^2 + 4\gamma\tau\|\delta_t^*\theta_{\boldsymbol{w}}^{n+1}\|^2 + C\tau h^{2r-2} + C\tau h^{2r} \\ &\le \frac{\tau}{2}\|\delta_t^*\xi_{\boldsymbol{u}}^{n+1}\|^2 + \tau^3\|\nabla\xi_p^{n+1}\|^2 + C\tau\|\tilde{\xi}_{\boldsymbol{u}}^{n+1}\|^2 + \gamma\tau\|\xi_{\boldsymbol{w}}^{n+1}\|^2 + C\tau h^{2r-2}, \end{aligned} \tag{64}$$

$$\begin{aligned} S_3 &\le 4C\nu\tau\|\delta_t^*\xi_{\boldsymbol{u}}^{n+1}\|((\|\nabla\hat{\boldsymbol{u}}^{*}(t_{n+1})\| + \|\nabla e_{\boldsymbol{u}}^{*,n}\|)\|\Delta\boldsymbol{u}(t_{n+1})\| \\ &\quad + \|\boldsymbol{u}_h^{*,n}\|_{L^\infty}\|\nabla\tilde{e}_{\boldsymbol{u}}^{n+1}\|) \\ &\le \frac{\tau}{2}\|\delta_t^*\xi_{\boldsymbol{u}}^{n+1}\|^2 + 4C\nu^2\tau\|\Delta\boldsymbol{u}(t_{n+1})\|^2(\|\nabla\hat{\boldsymbol{u}}^{*}(t_{n+1})\|^2 + \|\nabla\xi_{\boldsymbol{u}}^{n}\|^2 \\ &\quad + \|\nabla\xi_{\boldsymbol{u}}^{n-1}\|^2) + 4C\nu^2\tau\|\Delta\boldsymbol{u}(t_{n+1})\|^2(\|\nabla\theta_{\boldsymbol{u}}^{n}\|^2 + \|\nabla\theta_{\boldsymbol{u}}^{n-1}\|^2) \\ &\quad + 4C\nu^2\tau\|\boldsymbol{u}_h^{*,n}\|_{L^\infty}^2(\|\nabla\theta_{\boldsymbol{u}}^{n+1}\| + \|\nabla\tilde{\xi}_{\boldsymbol{u}}^{n+1}\|) \\ &\le \frac{\tau}{2}\|\delta_t^*\xi_{\boldsymbol{u}}^{n+1}\|^2 + C\tau(\|\nabla\tilde{\xi}_{\boldsymbol{u}}^{n+1}\|^2 + \|\nabla\xi_{\boldsymbol{u}}^{n}\|^2 + \|\nabla\xi_{\boldsymbol{u}}^{n-1}\|^2) + C\tau^5 + C\tau h^{2r}, \end{aligned} \tag{65}$$

$$\begin{aligned} S_4 &\le 4\beta\tau\|\delta_t^*\xi_{\boldsymbol{u}}^{n+1}\|(\|\boldsymbol{u}_h^{*,n}\|_{L^\infty}^2\|\tilde{e}_{\boldsymbol{u}}^{n+1}\| + \|\Delta\boldsymbol{u}^{**}(t_{n+1})\|\|\Delta\boldsymbol{u}(t_{n+1})\|\|\hat{\boldsymbol{u}}^{*}(t_{n+1})\| \\ &\quad + (\|\Delta\boldsymbol{u}^{*}(t_n)\| + \|\boldsymbol{u}_h^{*,n}\|_{L^\infty})\|\Delta\boldsymbol{u}(t_{n+1})\|\|e_{\boldsymbol{u}}^{*,n}\|) \\ &\le \frac{\tau}{2}\|\delta_t^*\xi_{\boldsymbol{u}}^{n+1}\|^2 + 4C\beta^2\tau(\|\theta_{\boldsymbol{u}}^{*,n}\|^2 + \|\theta_{\boldsymbol{u}}^{n+1}\|^2 + \|\tilde{\xi}_{\boldsymbol{u}}^{n+1}\|^2 \\ &\quad + \|\xi_{\boldsymbol{u}}^{n}\|^2 + \|\xi_{\boldsymbol{u}}^{n-1}\|^2) + C\tau^5 \\ &\le \frac{\tau}{2}\|\delta_t^*\xi_{\boldsymbol{u}}^{n+1}\|^2 + 4C\beta^2\tau(\|\tilde{\xi}_{\boldsymbol{u}}^{n+1}\|^2 + \|\xi_{\boldsymbol{u}}^{n}\|^2 + \|\xi_{\boldsymbol{u}}^{n-1}\|^2) \\ &\quad + C\tau h^{2(r+1)} + C\tau^5. \end{aligned} \tag{66}$$

Substituting (64)-(66) into (63) and summing it over n from 1 to m, we get

$$\begin{aligned} &\mu(\|\nabla\xi_{\boldsymbol{u}}^{m+1}\|^2 + \|2\nabla\xi_{\boldsymbol{u}}^{m+1} - \nabla\xi_{\boldsymbol{u}}^{m}\|^2) + \gamma(\|\xi_{\boldsymbol{w}}^{m+1}\|^2 + \|2\xi_{\boldsymbol{w}}^{m+1} - \xi_{\boldsymbol{w}}^{m}\|^2) \\ &\quad + \sum_{n=1}^{m}(2\tau\|\delta_t^*\xi_{\boldsymbol{u}}^{n+1}\|^2 + \mu\|\nabla\hat{\xi}_{\boldsymbol{u}}^{*,n+1}\|^2 + \|\hat{\xi}_{\boldsymbol{w}}^{*,n+1}\|^2 + \|\hat{\xi}_{\boldsymbol{u}}^{*,n+1}\|^2) \\ &\le C\tau\sum_{n=1}^{m}(\|\nabla\tilde{\xi}_{\boldsymbol{u}}^{n+1}\|^2 + \|\nabla\xi_{\boldsymbol{u}}^{n}\|^2 + \|\nabla\xi_{\boldsymbol{u}}^{n-1}\|^2 + \|\tilde{\xi}_{\boldsymbol{u}}^{n+1}\|^2 + \|\xi_{\boldsymbol{u}}^{n}\|^2 + \|\xi_{\boldsymbol{u}}^{n-1}\|^2 \\ &\quad + \tau^2\|\nabla\xi_p^{n+1}\|^2 + \|\xi_{\boldsymbol{w}}^{n+1}\|^2) + Ch^{2r-2} + C\tau^4. \end{aligned} \tag{67}$$

Employing the discrete Gronwall's inequality, we obtain

$$\begin{aligned} &\mu(\|\nabla\xi_{\boldsymbol{u}}^{m+1}\|^2 + \|2\nabla\xi_{\boldsymbol{u}}^{m+1} - \nabla\xi_{\boldsymbol{u}}^{m}\|^2) + \gamma(\|\xi_{\boldsymbol{w}}^{m+1}\|^2 + \|2\xi_{\boldsymbol{w}}^{m+1} - \xi_{\boldsymbol{w}}^{m}\|^2) \\ &\quad + \sum_{n=1}^{m}(2\tau\|\delta_t^*\xi_{\boldsymbol{u}}^{n+1}\|^2 + \mu\|\nabla\hat{\xi}_{\boldsymbol{u}}^{*,n+1}\|^2 + \|\hat{\xi}_{\boldsymbol{w}}^{*,n+1}\|^2 + \|\hat{\xi}_{\boldsymbol{u}}^{*,n+1}\|^2) \\ &\le C(h^{2r-2} + \tau^4). \end{aligned} \tag{68}$$

Subsequently, we choose $\boldsymbol{v}_h = 4\tau\tilde{\xi}_{\boldsymbol{w}}^{n+1}$ in (39a) and have

$$
\begin{aligned}
&(3\tilde{\xi}_{\boldsymbol{u}}^{n+1} - 4\xi_{\boldsymbol{u}}^{n} + \xi_{\boldsymbol{u}}^{n-1}, 2\tilde{\xi}_{\boldsymbol{w}}^{n+1}) + 4\mu\tau(\nabla\tilde{\xi}_{\boldsymbol{u}}^{n+1}, \nabla\tilde{\xi}_{\boldsymbol{w}}^{n+1}) + 4\gamma\tau\|\nabla\tilde{\xi}_{\boldsymbol{w}}^{n+1}\|^2 \\
&\quad + 4\alpha\tau(\tilde{\xi}_{\boldsymbol{u}}^{n+1}, \tilde{\xi}_{\boldsymbol{w}}^{n+1}) + 4\tau(\nabla e_p^n, \tilde{\xi}_{\boldsymbol{w}}^{n+1}) \\
&= 4\tau(R_{\boldsymbol{u}}^{n+1}, \tilde{\xi}_{\boldsymbol{w}}^{n+1}) - 4\tau(\delta_t^*\theta_{\boldsymbol{u}}^{n+1}, \tilde{\xi}_{\boldsymbol{w}}^{n+1}) - 4\alpha\tau(\theta_{\boldsymbol{u}}^{n+1}, \tilde{\xi}_{\boldsymbol{w}}^{n+1}) \\
&\quad - 4\nu\tau b(\hat{\boldsymbol{u}}^{*,n+1}, \boldsymbol{u}^{n+1}, \tilde{\xi}_{\boldsymbol{w}}^{n+1}) - 4\nu\tau b(e_{\boldsymbol{u}}^{*,n}, \boldsymbol{u}^{n+1}, \tilde{\xi}_{\boldsymbol{w}}^{n+1}) \\
&\quad - 4\nu\tau b(\boldsymbol{u}_h^{*,n}, \tilde{e}_{\boldsymbol{u}}^{n+1}, \tilde{\xi}_{\boldsymbol{w}}^{n+1}) - 4\beta\tau(|\boldsymbol{u}_h^{*,n}|^2\tilde{e}_{\boldsymbol{u}}^{n+1}, \tilde{\xi}_{\boldsymbol{w}}^{n+1}) \\
&\quad - 4\beta\tau((\boldsymbol{u}^{**,n+1}\cdot\hat{\boldsymbol{u}}^{*,n+1})\boldsymbol{u}^{n+1}, \tilde{\xi}_{\boldsymbol{w}}^{n+1}) - 4\tau(\nabla(p^{n+1}-p^n), \tilde{\xi}_{\boldsymbol{w}}^{n+1}) \\
&\quad - 4\beta\tau((\boldsymbol{u}^{*,n} + \boldsymbol{u}_h^{*,n})\cdot e_{\boldsymbol{u}}^{*,n}\boldsymbol{u}^{n+1}, \tilde{\xi}_{\boldsymbol{w}}^{n+1}).
\end{aligned} \tag{69}
$$

Taking $\boldsymbol{\phi}_h = 4\mu\tau\tilde{\xi}_{\boldsymbol{w}}^{n+1}$ and $4\alpha\tau\tilde{\xi}_{\boldsymbol{u}}^{n+1}$ in (39b), we obtain

$$
4\mu\tau(\nabla\tilde{\xi}_{\boldsymbol{u}}^{n+1}, \nabla\tilde{\xi}_{\boldsymbol{w}}^{n+1}) = 4\mu\tau\|\tilde{\xi}_{\boldsymbol{w}}^{n+1}\|^2 + 4\mu\tau(\theta_{\boldsymbol{w}}^{n+1}, \tilde{\xi}_{\boldsymbol{w}}^{n+1}), \tag{70a}
$$

$$
4\alpha\tau(\tilde{\xi}_{\boldsymbol{u}}^{n+1}, \tilde{\xi}_{\boldsymbol{w}}^{n+1}) = 4\alpha\tau\|\nabla\tilde{\xi}_{\boldsymbol{u}}^{n+1}\|^2 - 4\alpha\tau(\theta_{\boldsymbol{w}}^{n+1}, \tilde{\xi}_{\boldsymbol{u}}^{n+1}). \tag{70b}
$$

Choosing $\boldsymbol{v}_h = 4\tau\tilde{\xi}_{\boldsymbol{w}}^{n+1}$ in (40), we derive

$$
\begin{aligned}
&(3e_{\boldsymbol{u}}^{n+1} - 3\tilde{e}_{\boldsymbol{u}}^{n+1}, 2\tilde{\xi}_{\boldsymbol{w}}^{n+1}) + 4\tau(\nabla(e_p^{n+1} - e_p^n), \tilde{\xi}_{\boldsymbol{w}}^{n+1}) \\
&= 4\tau(\nabla(p^{n+1}-p^n), \tilde{\xi}_{\boldsymbol{w}}^{n+1}).
\end{aligned} \tag{71}
$$

Taking $\boldsymbol{\phi}_h = 2(3\xi_{\boldsymbol{u}}^{n+1} - 4\xi_{\boldsymbol{u}}^{n} + \xi_{\boldsymbol{u}}^{n-1})$ in (59a), $\boldsymbol{\phi}_h = \delta_t^* e_{\boldsymbol{u}}^{n+1}$ in (59b), $q_h = 4\tau\Delta(p_h^{n+1} - p_h^n)$ in (59d) and $\boldsymbol{v}_h = \frac{8\tau^2}{3}\Delta\delta_t^* e_{\boldsymbol{u}}^{n+1}$ in (40), we have

$$
\begin{aligned}
&(3\xi_{\boldsymbol{u}}^{n+1} - 4\xi_{\boldsymbol{u}}^{n} + \xi_{\boldsymbol{u}}^{n-1}, 2\tilde{\xi}_{\boldsymbol{w}}^{n+1}) \\
&= (3\xi_{\boldsymbol{u}}^{n+1} - 4\xi_{\boldsymbol{u}}^{n} + \xi_{\boldsymbol{u}}^{n-1}, 2\xi_{\boldsymbol{w}}^{n+1}) + (3\xi_{\boldsymbol{u}}^{n+1} - 4\xi_{\boldsymbol{u}}^{n} + \xi_{\boldsymbol{u}}^{n-1}, 2\tilde{\xi}_{\boldsymbol{w}}^{n+1} - 2\xi_{\boldsymbol{w}}^{n+1}) \\
&= (3\xi_{\boldsymbol{u}}^{n+1} - 4\xi_{\boldsymbol{u}}^{n} + \xi_{\boldsymbol{u}}^{n-1}, 2\xi_{\boldsymbol{w}}^{n+1} + 2\theta_{\boldsymbol{w}}^{n+1}) \\
&\quad - 4\tau(\delta_t^*\xi_{\boldsymbol{u}}^{n+1}, \theta_{\boldsymbol{w}}^{n+1}) + 4\tau(\delta_t^* e_{\boldsymbol{u}}^{n+1}, \tilde{\xi}_{\boldsymbol{w}}^{n+1} - \xi_{\boldsymbol{w}}^{n+1}) - 4\tau(\delta_t^*\theta_{\boldsymbol{u}}^{n+1}, \tilde{\xi}_{\boldsymbol{w}}^{n+1} - \xi_{\boldsymbol{w}}^{n+1}) \\
&= \|\nabla\xi_{\boldsymbol{u}}^{n+1}\|^2 - \|\nabla\xi_{\boldsymbol{u}}^{n}\|^2 + \|2\nabla\xi_{\boldsymbol{u}}^{n+1} - \nabla\xi_{\boldsymbol{u}}^{n}\|^2 - \|2\nabla\xi_{\boldsymbol{u}}^{n} - \nabla\xi_{\boldsymbol{u}}^{n-1}\|^2 \\
&\quad + \|\nabla\hat{\xi}_{\boldsymbol{u}}^{*,n+1}\|^2 - 4\tau(\theta_{\boldsymbol{w}}^{n+1}, \delta_t^*\xi_{\boldsymbol{u}}^{n+1}) - 4\tau(\delta_t^*\theta_{\boldsymbol{u}}^{n+1}, \tilde{\xi}_{\boldsymbol{w}}^{n+1} - \xi_{\boldsymbol{w}}^{n+1}).
\end{aligned} \tag{72}
$$

Choosing $q_h = \frac{8\tau^2}{3}\nabla(\Delta\xi_p^{n+1})$ in (40), one can easily get

$$
\begin{aligned}
&4\tau(\tilde{\xi}_{\boldsymbol{w}}^{n+1}, \nabla\xi_p^{n+1}) \\
&= \frac{4\tau^2}{3}(\|\Delta\xi_p^{n+1}\|^2 - \|\Delta\xi_p^{n}\|^2 + \|\Delta\xi_p^{n+1} - \Delta\xi_p^{n}\|^2) - 4\tau(\theta_{\boldsymbol{w}}^{n+1}, \nabla\xi_p^{n+1}) \\
&\quad + \frac{8\tau^2}{3}(\int_{t_n}^{t_{n+1}}\Delta\theta_{pt}dt, \Delta\xi_p^{n+1}) - \frac{8\tau^2}{3}(\int_{t_n}^{t_{n+1}}\Delta p_t dt, \Delta\xi_p^{n+1}).
\end{aligned} \tag{73}
$$

Substituting (69)-(73) into (67), we get

$$
\begin{aligned}
&\|\nabla\xi_{\boldsymbol{u}}^{n+1}\|^2 - \|\nabla\xi_{\boldsymbol{u}}^{n}\|^2 + \|2\nabla\xi_{\boldsymbol{u}}^{n+1} - \nabla\xi_{\boldsymbol{u}}^{n}\|^2 - \|2\nabla\xi_{\boldsymbol{u}}^{n} - \nabla\xi_{\boldsymbol{u}}^{n-1}\|^2 \\
&+ \|\nabla\hat{\xi}_{\boldsymbol{u}}^{*,n+1}\|^2 + 4\mu\tau\|\tilde{\xi}_{\boldsymbol{w}}^{n+1}\|^2 + 4\gamma\tau\|\nabla\tilde{\xi}_{\boldsymbol{w}}^{n+1}\|^2 + 4\alpha\tau\|\nabla\tilde{\xi}_{\boldsymbol{u}}^{n+1}\|^2 \\
&+ \frac{4\tau^2}{3}\|\Delta\xi_p^{n+1}\|^2 - \frac{4\tau^2}{3}\|\Delta\xi_p^{n}\|^2 + \frac{4\tau^2}{3}\|\Delta\xi_p^{n+1} - \Delta\xi_p^{n}\|^2 = \sum_{i=1}^{5} D_i,
\end{aligned} \tag{74}
$$

with

$$
\begin{aligned}
&D_1 = 4\tau(R_{\boldsymbol{u}}^{n+1}, \tilde{\xi}_{\boldsymbol{w}}^{n+1}), \\
&D_2 = -4\tau(\delta_t^*\theta_{\boldsymbol{u}}^{n+1}, \xi_{\boldsymbol{w}}^{n+1}) - 4\mu\tau(\theta_{\boldsymbol{w}}^{n+1}, \tilde{\xi}_{\boldsymbol{w}}^{n+1}) + 4\alpha\tau(\theta_{\boldsymbol{w}}^{n+1}, \tilde{\xi}_{\boldsymbol{u}}^{n+1}) + 4\tau(\theta_{\boldsymbol{w}}^{n+1}, \delta_t^*\xi_{\boldsymbol{u}}^{n+1})
\end{aligned}
$$

$$
\begin{aligned}
&- 4\alpha\tau(\theta_{\boldsymbol{u}}^{n+1}, \tilde{\xi}_{\boldsymbol{w}}^{n+1}) + 4\tau(\theta_{\boldsymbol{w}}^{n+1}, \nabla\xi_p^{n+1}) + 4\tau(\theta_p^{n+1}, \nabla\cdot\tilde{\xi}_{\boldsymbol{w}}^{n+1}),\\
D_3 &= -4\nu\tau b(\hat{\boldsymbol{u}}^{*,n+1}, \boldsymbol{u}^{n+1}, \tilde{\xi}_{\boldsymbol{w}}^{n+1}) - 4\nu\tau b(e_{\boldsymbol{u}}^{*,n}, \boldsymbol{u}^{n+1}, \tilde{\xi}_{\boldsymbol{w}}^{n+1}) - 4\nu\tau b(\boldsymbol{u}_h^{*,n}, \tilde{e}_{\boldsymbol{u}}^{n+1}, \tilde{\xi}_{\boldsymbol{w}}^{n+1}),\\
D_4 &= -4\beta\tau(|\boldsymbol{u}_h^{*,n}|^2\tilde{e}_{\boldsymbol{u}}^{n+1}, \tilde{\xi}_{\boldsymbol{w}}^{n+1}) - 4\beta\tau((\boldsymbol{u}^{*,n} + \boldsymbol{u}_h^{*,n})\cdot e_{\boldsymbol{u}}^{*,n}\boldsymbol{u}^{n+1}, \tilde{\xi}_{\boldsymbol{w}}^{n+1})\\
&\quad - 4\beta\tau((\boldsymbol{u}^{**,n+1}\cdot\hat{\boldsymbol{u}}^{*,n+1})\boldsymbol{u}^{n+1}, \tilde{\xi}_{\boldsymbol{w}}^{n+1}),\\
D_5 &= \frac{8\tau^2}{3}(\int_{t_n}^{t_{n+1}} \Delta p_t dt, \Delta\xi_p^{n+1}) - \frac{8\tau^2}{3}(\int_{t_n}^{t_{n+1}} \Delta\theta_{pt} dt, \Delta\xi_p^{n+1}).
\end{aligned}
$$

By using the Lemma 4.1, integration by parts, Hölder's inequality, Young's inequality and $\tau \sim h^2$, we estimate the righthand side of (74) and obtain

$$
\begin{aligned}
(75)\quad D_1 &\le 4\tau\|R_{\boldsymbol{u}}^{n+1}\|\|\tilde{\xi}_{\boldsymbol{w}}^{n+1}\| \le \mu\tau\|\tilde{\xi}_{\boldsymbol{w}}^{n+1}\|^2 + \frac{4\tau}{\mu}\|R_{\boldsymbol{u}}^{n+1}\|^2 \le \mu\tau\|\tilde{\xi}_{\boldsymbol{w}}^{n+1}\|^2 + C\tau^5,\\
(76)\quad D_2 &\le 4\tau(\|\delta_t^*\theta_{\boldsymbol{u}}^{n+1}\|\|\tilde{\xi}_{\boldsymbol{w}}^{n+1}\| + \mu\|\theta_{\boldsymbol{w}}^{n+1}\|\|\tilde{\xi}_{\boldsymbol{w}}^{n+1}\| + \alpha\|\theta_{\boldsymbol{w}}^{n+1}\|\|\tilde{\xi}_{\boldsymbol{u}}^{n+1}\|\\
&\quad + \|\delta_t^*\xi_{\boldsymbol{u}}^{n+1}\|\|\theta_{\boldsymbol{w}}^{n+1}\| + \alpha\|\theta_{\boldsymbol{u}}^{n+1}\|\|\tilde{\xi}_{\boldsymbol{w}}^{n+1}\| + C\|\theta_{\boldsymbol{w}}^{n+1}\|\|\nabla\xi_p^{n+1}\|\\
&\quad + \|\theta_p^{n+1}\|\|\nabla\tilde{\xi}_{\boldsymbol{w}}^{n+1}\|)\\
&\le \gamma\tau\|\xi_{\boldsymbol{w}}^{n+1}\|^2 + \mu\tau\|\tilde{\xi}_{\boldsymbol{w}}^{n+1}\|^2 + \gamma\tau\|\nabla\tilde{\xi}_{\boldsymbol{w}}^{n+1}\|^2 + \frac{\tau}{2}\|\delta_t^*\xi_{\boldsymbol{u}}^{n+1}\|^2 + \tau^3\|\nabla\xi_p^{n+1}\|^2\\
&\quad + \alpha\tau\|\tilde{\xi}_{\boldsymbol{u}}^{n+1}\|^2 + C\tau(\|\delta_t^*\theta_{\boldsymbol{u}}^{n+1}\|^2 + \|\theta_{\boldsymbol{w}}^{n+1}\|^2 + \tau^{-2}\|\theta_{\boldsymbol{w}}^{n+1}\|^2\\
&\quad + \|\theta_{\boldsymbol{u}}^{n+1}\|^2 + \|\theta_p^{n+1}\|^2)\\
&\le \gamma\tau\|\xi_{\boldsymbol{w}}^{n+1}\|^2 + \mu\tau\|\tilde{\xi}_{\boldsymbol{w}}^{n+1}\|^2 + \gamma\tau\|\nabla\tilde{\xi}_{\boldsymbol{w}}^{n+1}\|^2 + \frac{\tau}{2}\|\delta_t^*\xi_{\boldsymbol{u}}^{n+1}\|^2 + \tau^3\|\nabla\xi_p^{n+1}\|^2\\
&\quad + \alpha\tau\|\tilde{\xi}_{\boldsymbol{u}}^{n+1}\|^2 + C\tau h^{2r-2},\\
(77)\quad D_3 &\le 4C\nu\tau\|\nabla\tilde{\xi}_{\boldsymbol{w}}^{n+1}\|(\|\nabla\hat{\boldsymbol{u}}^{*,n+1}\|\|\nabla\boldsymbol{u}^{n+1}\| + \|\nabla e_{\boldsymbol{u}}^{*,n}\|\|\nabla\boldsymbol{u}^{n+1}\|\\
&\quad + \|\boldsymbol{u}_h^{*,n}\|_{L^\infty}\|\nabla\tilde{e}_{\boldsymbol{u}}^{n+1}\|)\\
&\le \gamma\tau\|\nabla\tilde{\xi}_{\boldsymbol{w}}^{n+1}\|^2 + \frac{8C\nu^2}{\gamma}(\|\nabla\boldsymbol{u}^{n+1}\|^2(\|\nabla\hat{\boldsymbol{u}}^{*,n+1}\|^2 + \|\nabla\theta_{\boldsymbol{u}}^{n}\| + \|\nabla\theta_{\boldsymbol{u}}^{n-1}\|\\
&\quad + \|\nabla\xi_{\boldsymbol{u}}^{n}\| + \|\nabla\xi_{\boldsymbol{u}}^{n-1}\|) + \|\boldsymbol{u}_h^{*,n}\|_{L^\infty}^2(\|\nabla\theta_{\boldsymbol{u}}^{n+1}\| + \|\nabla\tilde{\xi}_{\boldsymbol{u}}^{n+1}\|))\\
&\le \gamma\tau\|\nabla\tilde{\xi}_{\boldsymbol{w}}^{n+1}\|^2 + C\tau(\|\nabla\tilde{\xi}_{\boldsymbol{u}}^{n+1}\|^2 + \|\nabla\xi_{\boldsymbol{u}}^{n}\| + \|\nabla\xi_{\boldsymbol{u}}^{n-1}\|) + C\tau(\tau^4 + h^{2r}),\\
(78)\quad D_4 &\le 4\beta\tau\|\nabla\tilde{\xi}_{\boldsymbol{w}}^{n+1}\|\big(\|\boldsymbol{u}_h^{*,n}\|_{L^\infty}^2(\|\nabla\theta_{\boldsymbol{u}}^{n+1}\| + \|\nabla\tilde{\xi}_{\boldsymbol{u}}^{n+1}\|)\\
&\quad + \|\Delta\boldsymbol{u}^{n+1}\|\|\nabla\boldsymbol{u}^{*,n+1}\|\|\boldsymbol{u}^{**,n+1}\| + \|\Delta\boldsymbol{u}^{n+1}\|(\|\nabla\boldsymbol{u}^{*,n}\| + \|\boldsymbol{u}_h^{*,n}\|_{L^\infty})\\
&\quad (\|\theta_{\boldsymbol{u}}^{n}\| + \|\xi_{\boldsymbol{u}}^{n}\| + \|\theta_{\boldsymbol{u}}^{n-1}\| + \|\xi_{\boldsymbol{u}}^{n-1}\|)\big)\\
&\le \gamma\tau\|\nabla\tilde{\xi}_{\boldsymbol{w}}^{n+1}\|^2 + \frac{12C\beta^2\tau}{\gamma}\big(\|\boldsymbol{u}_h^{*,n}\|_{L^\infty}^4(\|\nabla\theta_{\boldsymbol{u}}^{n+1}\|^2 + \|\nabla\tilde{\xi}_{\boldsymbol{u}}^{n+1}\|)\\
&\quad + \|\Delta\boldsymbol{u}^{n+1}\|^2\|\nabla\boldsymbol{u}^{*,n+1}\|^2\|\boldsymbol{u}^{**,n+1}\|^2 + \|\Delta\boldsymbol{u}^{n+1}\|^2(\|\nabla\boldsymbol{u}^{*,n}\|^2\\
&\quad + \|\boldsymbol{u}_h^{*,n}\|_{L^\infty}^2)(\|\theta_{\boldsymbol{u}}^{n}\|^2 + \|\xi_{\boldsymbol{u}}^{n}\|^2 + \|\theta_{\boldsymbol{u}}^{n-1}\|^2 + \|\xi_{\boldsymbol{u}}^{n-1}\|^2)\big)\\
&\le \gamma\tau\|\nabla\tilde{\xi}_{\boldsymbol{w}}^{n+1}\|^2 + C\tau(\|\nabla\tilde{\xi}_{\boldsymbol{u}}^{n+1}\| + \|\xi_{\boldsymbol{u}}^{n}\|^2 + \|\xi_{\boldsymbol{u}}^{n-1}\|^2) + C\tau h^{2r} + C\tau^5,\\
(79)\quad D_5 &\le \frac{8\tau^3}{3}\int_{t_n}^{t_{n+1}}(\|\Delta\theta_{pt}\| + \|\Delta p_t\|)ds\|\Delta\xi_p^{n+1}\| \le \tau^3\|\Delta\xi_p^{n+1}\|^2 + C\tau h^4.
\end{aligned}
$$

Substituting (75)-(79) into (74) and summing it over n from 1 to m, we deduce

$$\begin{aligned}
&\|\nabla\xi_{\boldsymbol{u}}^{m+1}\|^2+\|2\nabla\xi_{\boldsymbol{u}}^{m+1}-\nabla\xi_{\boldsymbol{u}}^{m}\|^2+\frac{4\tau^2}{3}\|\Delta\xi_p^{m+1}\|^2+\sum_{n=1}^{m}(\|\nabla\hat{\xi}_{\boldsymbol{u}}^{*,n+1}\|^2\\
&\quad+2\mu\tau\|\tilde{\xi}_{\boldsymbol{w}}^{n+1}\|^2+\gamma\tau\|\nabla\tilde{\xi}_{\boldsymbol{w}}^{n+1}\|^2+\alpha\tau\|\nabla\tilde{\xi}_{\boldsymbol{u}}^{n+1}\|^2+\frac{4\tau^2}{3}\|\Delta\xi_p^{n+1}-\Delta\xi_p^{n}\|^2)\\
&\le\frac{\tau}{2}\sum_{n=1}^{m}\|\delta_t^*\xi_{\boldsymbol{u}}^{n+1}\|^2+C\tau\sum_{n=1}^{m}(\tau^2\|\Delta\xi_p^{n+1}\|^2+\|\nabla\xi_{\boldsymbol{u}}^{n}\|^2+\|\nabla\xi_{\boldsymbol{u}}^{n-1}\|^2\\
&\quad+\|\nabla\tilde{\xi}_{\boldsymbol{u}}^{n+1}\|^2+\|\xi_{\boldsymbol{w}}^{n+1}\|^2)+C\tau(\max\{h^4,h^{2r-2}\}+\tau^4).
\end{aligned}\tag{80}$$

Employing the discrete Gronwall's inequality, we obtain

$$\begin{aligned}
&\|\nabla\xi_{\boldsymbol{u}}^{m+1}\|^2+\|2\nabla\xi_{\boldsymbol{u}}^{m+1}-\nabla\xi_{\boldsymbol{u}}^{m}\|^2+\frac{4\tau^2}{3}\|\Delta\xi_p^{m+1}\|^2+\sum_{n=1}^{m}(\|\nabla\hat{\xi}_{\boldsymbol{u}}^{*,n+1}\|^2\\
&\quad+2\mu\tau\|\tilde{\xi}_{\boldsymbol{w}}^{n+1}\|^2+\gamma\tau\|\nabla\tilde{\xi}_{\boldsymbol{w}}^{n+1}\|^2+\alpha\tau\|\nabla\tilde{\xi}_{\boldsymbol{u}}^{n+1}\|^2+\frac{4\tau^2}{3}\|\Delta\xi_p^{n+1}-\Delta\xi_p^{n}\|^2)\\
&\le C(\max\{h^4,h^{2r-2}\}+\tau^4).
\end{aligned}\tag{81}$$

Next, from the equation of (2), it is easy to get

$$\begin{aligned}
\|e_p^{n+1}\|&\le\beta^*\sup_{\boldsymbol{v}_h\in\boldsymbol{V}_h}\frac{(e_p^{n+1},\nabla\cdot\boldsymbol{v}_h)}{\|\nabla\boldsymbol{v}_h\|}\\
&\le\frac{\beta^*}{\|\nabla\boldsymbol{v}_h\|}\Big((\delta_t^*e_{\boldsymbol{u}}^{n+1},\boldsymbol{v}_h)+\mu(\nabla\tilde{e}_{\boldsymbol{u}}^{n+1},\nabla\boldsymbol{v}_h)+\gamma(\nabla\tilde{e}_{\boldsymbol{w}}^{n+1},\nabla\boldsymbol{v}_h)\\
&\quad+\nu b(\hat{\boldsymbol{u}}^*(t_{n+1}),\boldsymbol{u}(t_{n+1}),\boldsymbol{v}_h)+\nu b(e_{\boldsymbol{u}}^{*,n},\boldsymbol{u}(t_{n+1}),\boldsymbol{v}_h)\\
&\quad+\nu b(\boldsymbol{u}_h^{*,n},\tilde{e}_{\boldsymbol{u}}^{n+1},\boldsymbol{v}_h)+\alpha(\tilde{e}_{\boldsymbol{u}}^{n+1},\boldsymbol{v}_h)-(R_{\boldsymbol{u}}(t_{n+1}),\boldsymbol{v}_h)\\
&\quad+\beta(|\boldsymbol{u}_h^{*,n}|^2\tilde{e}_{\boldsymbol{u}}^{n+1},\boldsymbol{v}_h)+\beta((\boldsymbol{u}^*(t_n)+\boldsymbol{u}_h^{*,n}))\cdot e_{\boldsymbol{u}}^{*,n}\boldsymbol{u}(t_{n+1}),\boldsymbol{v}_h)\\
&\quad+\beta(\boldsymbol{u}^{**}(t_{n+1})\cdot\hat{\boldsymbol{u}}^*(t_{n+1})\boldsymbol{u}(t_{n+1}),\boldsymbol{v}_h)\Big)\\
&\le C(\tau^2+\|\delta_t^*e_{\boldsymbol{u}}^{n+1}\|+\|\nabla\tilde{e}_{\boldsymbol{u}}^{n+1}\|+\|\nabla\tilde{e}_{\boldsymbol{w}}^{n+1}\|+\|e_{\boldsymbol{u}}^{n}\|+\|e_{\boldsymbol{u}}^{n-1}\|).
\end{aligned}\tag{82}$$

Square both sides of (82) and multiplying by τ, then summing over n from 1 to m, it holds

$$\begin{aligned}
\tau\sum_{n=1}^{m}\|e_p^{n+1}\|^2\le C\tau\sum_{n=1}^{m}(&\tau^4+\|\delta_t^*e_{\boldsymbol{u}}^{n+1}\|^2+\|\nabla\tilde{e}_{\boldsymbol{u}}^{n+1}\|^2+\|\nabla\tilde{e}_{\boldsymbol{w}}^{n+1}\|^2\\
&+\|e_{\boldsymbol{u}}^{n}\|^2+\|e_{\boldsymbol{u}}^{n-1}\|^2).
\end{aligned}\tag{83}$$

Finally, we are able to derive the desired result (38) by using the equations of (56), (68), (81), (83) and triangle inequality.

□

Remark 4.1. If choosing $\tau\sim h^{\frac{3}{2}}$ in (54), (64), (76) and (79), we can obtain the error estimates as follows:

Theorem 4.1. Let $(\tilde{\boldsymbol{u}}_h^m,\tilde{\boldsymbol{w}}_h^m,\boldsymbol{u}_h^m,p_h^m)$ and $(\boldsymbol{u}(t_m),\boldsymbol{w}(t_m),p(t_m))$ be the solutions of (13)-(15) and (6), respectively. Under Lemma 4.1, the Assumption (35)

and $\tau \sim h^{\frac{3}{2}}$, then for all $0 \leq m \leq N$, we have

$$\begin{aligned} &\|e_{\boldsymbol{u}}^{m+1}\|^2 + \|e_{\boldsymbol{u}}^{*,m+1}\|^2 + \|\nabla e_{\boldsymbol{u}}^{m+1}\|^2 + \tau\sum_{n=1}^{m}\|e_p^{n+1}\|^2 \\ &\leq C(\tau^4 + \max\{h^{2r-1}, h^3\}). \end{aligned} \tag{84}$$

5. Numerical experiments

In this section, we present a battery of numerical experiments to solve the active fluid model by implementing the developed scheme (13)-(15), where the stable $\boldsymbol{P}_2$-$\boldsymbol{P}_2$-P_1 elements are used for the velocity $\boldsymbol{u}$, auxiliary variable $\boldsymbol{w}$ and pressure p. The numerical examples include the stability/accuracy tests and the some simulations of self-organization. Our computations are done using the software package FreeFem++ [13] and the computational domain is set as $\Omega = [0,1]^d$.

5.1. Convergence and stability tests. We first verify the temporal and spatial convergence of the proposed scheme, where the domain is set as $\Omega = [0,1]^2$. The initial condition reads as

$$\boldsymbol{u}_0(\boldsymbol{x}) = (-(\cos(2\pi x + \pi) + 1)\sin(2\pi y), (\cos(2\pi y + \pi) + 1)\sin(2\pi x)).$$

Then, the external body force is given by $\boldsymbol{f}(\boldsymbol{x}, t) = (0, 0)$, and the model parameters are set as follows $\mu = \nu = \beta = \alpha = 0.1$ and $\gamma = 0.01$.

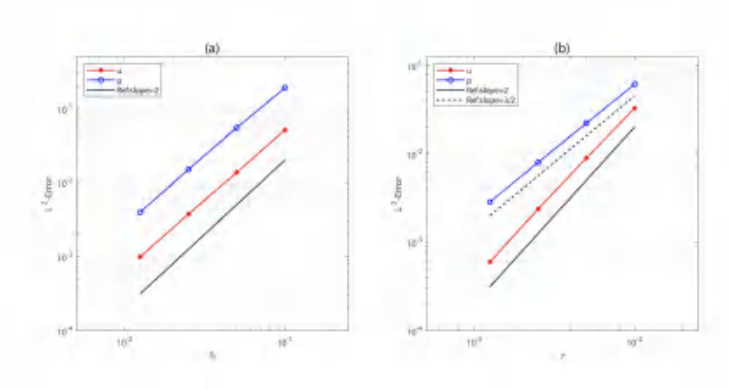

FIGURE 1. The L^2 errors for the velocity field $\boldsymbol{u}$ and pressure p at time $t = 1$, where (a) convergence order in space, and (b) convergence order in time.

Due to the exact solutions are not known when deriving the rates of numerical convergence, the exact solutions are computed employing the temporal step size $\tau = 1/10000$ and the spatial mesh size $h = 1/120$. Subsequently, to testify convergence rates of spatial errors for the velocity and pressure, we fix the temporal step size $\tau = 1/1000$ and calculate the numerical errors with the following spatial mesh sizes $h = 1/10$, $1/20$, $1/40$ and $1/80$ at $t = 1$. Figure 1 (a) demonstrates that the convergence rates of L^2-norm of pressure p and H^1-norm of velocity field $\boldsymbol{u}$ are closer to theoretical convergence rates $\mathcal{O}(h^2)$. Next, in order to verify the temporal convergence rates of $\mathcal{O}(\tau^2)$ for L^2-norm of velocity field and pressure respectively, the spatial mesh size $h = 1/80$ is fixed and different temporal step sizes $\tau = 1/100$, $1/200$, $1/400$ and $1/800$ are utilized to compute the errors. Figure 1 (b) exhibits the computational results, which are consistent with the theoretical prediction.

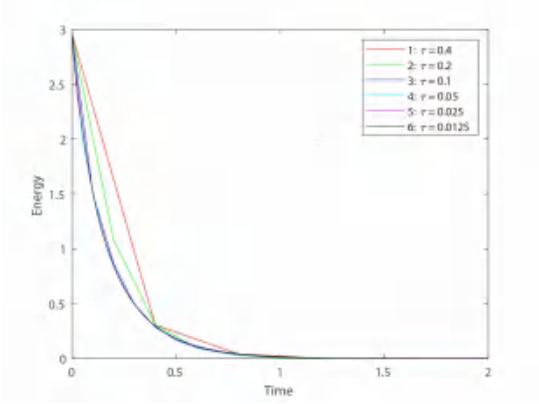

FIGURE 2. Time evolution of the total energy functional E_{tot}^n for $\tau = 0.4$, 0.2, 0.1, 0.05, 0.025 and 0.0125.

In Figure 2, we further verify the energy stability of the stabilized pressure-projection scheme. We consider the parameters $\mu = 0.045$, $\nu = 0.003$, $\beta = 0.5$, $\alpha = -0.81$ and $\gamma = \mu^3$, and a fixed spatial mesh size of $h = 1/50$. The energy evolution curves are plotted for different time steps $\tau = 0.4$, 0.2, 0.1, 0.05, 0.025 and 0.0125, up to the final time $T = 2$. As can be seen from the obtained energy curves, the fully discrete numerical scheme is stable for the different temporal step sizes and the energy eventually tends to 0 over time.

TABLE 1. The numerical errors and spatial convergence orders at $t = 1$.

h	$\|\boldsymbol{u} - \boldsymbol{u}_h^m\|$	order	$\|p - p_h^m\|$	order	$\|\boldsymbol{u} - \boldsymbol{u}_h^m\|^*$	order	$\|p - p_h^m\|^*$	order
1/10	5.30e-04	-	1.30e-03	-	4.94e-06	-	1.92e-06	-
1/20	2.16e-04	1.28	5.31e-04	1.32	5.79e-07	3.09	4.79e-07	2.00
1/40	7.42e-05	1.54	1.73e-04	1.61	7.91e-08	2.87	1.24e-07	1.94
1/80	1.99e-05	1.89	5.02e-05	1.78	9.61e-09	3.04	3.06e-08	2.02

In addition, we compare the L^2-norm errors and spatial convergence orders of velocity field $\boldsymbol{u}$ and pressure p with and without the addition of the auxiliary variable $\boldsymbol{w} = -\Delta \boldsymbol{u}$ through another initial condition. The initial condition for $\boldsymbol{u}$ is given by

$$\boldsymbol{u}_0 = (\sin^2(\pi x)\sin(\pi y)\cos(\pi y), -\sin^2(\pi y)\sin(\pi x)\cos(\pi x)).$$

The parameters are set the same as in convergence test. Table 1 shows the spatial error and the convergence order, where the errors and the orders of convergence without the addition of auxiliary variables are shown with $\|\cdot\|$, and the errors and the orders of convergence with the addition of auxiliary variables are marked with $\|\cdot\|^*$. The results show that with the addition of the auxiliary variable, the errors of velocity and pressure are smaller, and the order of convergence is better.

5.2. Self-organization of active fluid in 2D. In this subsection, we simulate the self-organization of active fluid in 2D by the stabilized pressure-projection scheme. In Figures 3 and 4, the spatial self-organization of the bacterial active fluid was observed by adding purified genomic DNA to the dense active suspension of Escherichia coli cells, see [21]. Figures 3 and 4 show the phase space trajectory

of the bacterial active fluid rotating clockwise or counterclockwise at a constant angle to form a unidirectional vortex current and the fluid rate reversing, respectively. These fascinating patterns are created by the self-organization of active fluid and can be affected by external disturbances. Moreover, experiments involving the self-organization of active fluid can provide valuable insights into aspects such as material preparation and biofilm formation.

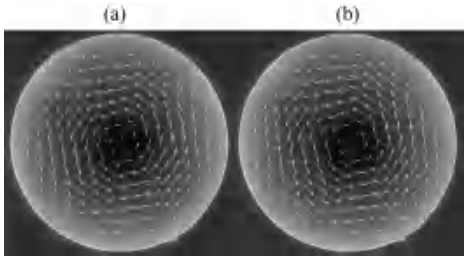

FIGURE 3. Phase-contrast image and instantaneous velocity field of a unidirectional giant vortex, snapshots are taken at (a) t=10.00 and (b) t=22.00 (https://static-content.springer.com/esm/art%3A10.1038%2Fs41586-020-03168-6/MediaObjects/41586_2020_3168_MOESM2_ESM.mp4).

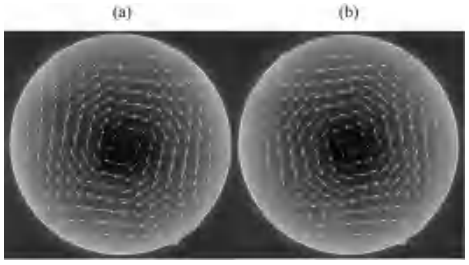

FIGURE 4. Phase-contrast image and instantaneous velocity field of giant vortices with variable direction, snapshots are taken at (a) t=10.00 and (b) t=22.00 (https://static-content.springer.com/esm/art%3A10.1038%2Fs41586-020-03168-6/MediaObjects/41586_2020_3168_MOESM3_ESM.mp4).

In what follows, we use the scheme (13)-(15) to simulate the real biological self-organization in Figures 3 and 4. Now, we consider the computational domain as $\boldsymbol{x} \in \Omega = [0,1]^2$ and the initial condition as

$$\boldsymbol{u}_0(\boldsymbol{x}) = (\text{rand}(x,y), \text{rand}(x,y)),$$

where $\text{rand}(x,y)$ represents the random number in the interval $[-1,1]$ and follows a normal distribution. The boundary conditions satisfy $\boldsymbol{u}|_{\partial\Omega} = 0$, and parameters of the model are set as follows: $\mu = 0.045$, $\nu = 0.003$, $\beta = 0.5$, $\alpha = -0.81$ and $\gamma = \mu^3$. To better show the simulation results, we set the computational time $t \in [0,2]$ and $\tau = 1/1000$.

Firstly, we set the external body force $\boldsymbol{f}(\boldsymbol{x},t) = (0,0)$. Under different random initial conditions, active fluid forms a polar ordered state over time. We choose a random initial condition and find that there is only one vortex in the computational

domain after $t = 0.10$. As time goes by, the collective direction of the active fluid remains counterclockwise, and the velocity of the active fluid tends to 0. Figure 5 shows the snapshots of $\boldsymbol{u}$ at $t = 0.00$, 0.01, 0.10 and 1.00. For each subfigure, the left and the right are direction and magnitude(indicated by the colourmap) of collective velocity, respectively. In Figure 5(a), one can clearly see the highly disordered distribution of the magnitude and direction of the active fluid. Figure 5(b) show the active fluid forms the vortices with disordered distribution. Eventually, the active fluid forms a polar ordered state, as shown in Figures 5(c)-(d). Here, the presence of the second nonlinearity in the system provides additional freedom, enabling the system to self-organize into a polar order state without the need for external fine-tuning.

Secondly, we set the driving force

$$\boldsymbol{f}(\boldsymbol{x},t) = \begin{cases} ((\cos(2\pi x+\pi)+1)\times\sin(2\pi y), (\cos(2\pi y+\pi)+1))\times\sin(2\pi x), \\ \quad (x,y)\in\left(\frac{1}{4},\frac{3}{4}\right)\times\left(\frac{1}{4},\frac{3}{4}\right),\ t\in\left[k,k+\frac{1}{2}\right), k=0,1,2,\cdots, \\ ((\cos(2\pi x+\pi)+1)\times\sin(2\pi y), -(\cos(2\pi y+\pi)+1)\times\sin(2\pi x)), \\ \quad (x,y)\in\left(\frac{1}{4},\frac{3}{4}\right)\times\left(\frac{1}{4},\frac{3}{4}\right),\ t\in\left[k+\frac{1}{2},k+1\right), k=0,1,2,\cdots. \end{cases}$$

The snapshots of $\boldsymbol{u}$ at $t = 0.00$, 0.50, 0.72 and 1.00 are shown in Figure 6. In Figure 6(a), it is clear that the magnitude and direction of the active fluid are highly disordered distribution. Figure 6(b) shows the active fluid forms a polar ordered state and the collective direction is clockwise. We observe that the collective direction of the active fluid becomes counterclockwise in Figures 6(c)-(d). Here, the temporally periodic driving force reverses the collective direction of the active fluid periodically.

Figures 5 and 6 show the phase space trajectory of the active fluid rotating counterclockwise to form a unidirectional vortex current, and the phase space trajectory of the active fluid moving direction with periodic reversal, respectively. We observed that this is well consistent with the experimental observations in Figures 3 and 4, and find that the direction of motion of the active fluid can be changed by changing the external body force $\boldsymbol{f}(\boldsymbol{x},t)$. Then we set the different external body forces $\boldsymbol{f}(\boldsymbol{x},t)$ to investigate the difference phenomena of the active fluid.

Next, the external body force and the initial condition are set as $\boldsymbol{f}(\boldsymbol{x},t) = (\cos(2\pi y), \cos(2\pi x))$ and the random number in $[-1,1]$ with the normal distribution, respectively. We show the snapshots of $\boldsymbol{u}$ at $t = 0.00$, 0.01, 0.10 and 1.00. As can be seen from Figures 7(a) and (b), the active fluid begins to form the vortices with disordered distribution through self-organization. Driven by external body force and self-organized by active fluid, the disordered vortices in the region gradually merge into a large vortex and a small vortex over time, as shown in Figure 7(c). Finally, it can be seen from Figure 7(d) that the large vortex and the small vortex form two symmetrical vortices of the same size and opposite directions.

5.3. Self-organization of active fluid in 3D. We will now proceed with 3D simulations. The computed domain is set as $\boldsymbol{x}\in\Omega = [0,1]^3$ and the initial condition reads as

$$\boldsymbol{u}_0(\boldsymbol{x}) = (\mathrm{rand}(x,y,z), \mathrm{rand}(x,y,z), \mathrm{rand}(x,y,z)).$$

Then we change the external body force $\boldsymbol{f}(\boldsymbol{x},t)$ to investigate the difference phenomena of the active fluid.

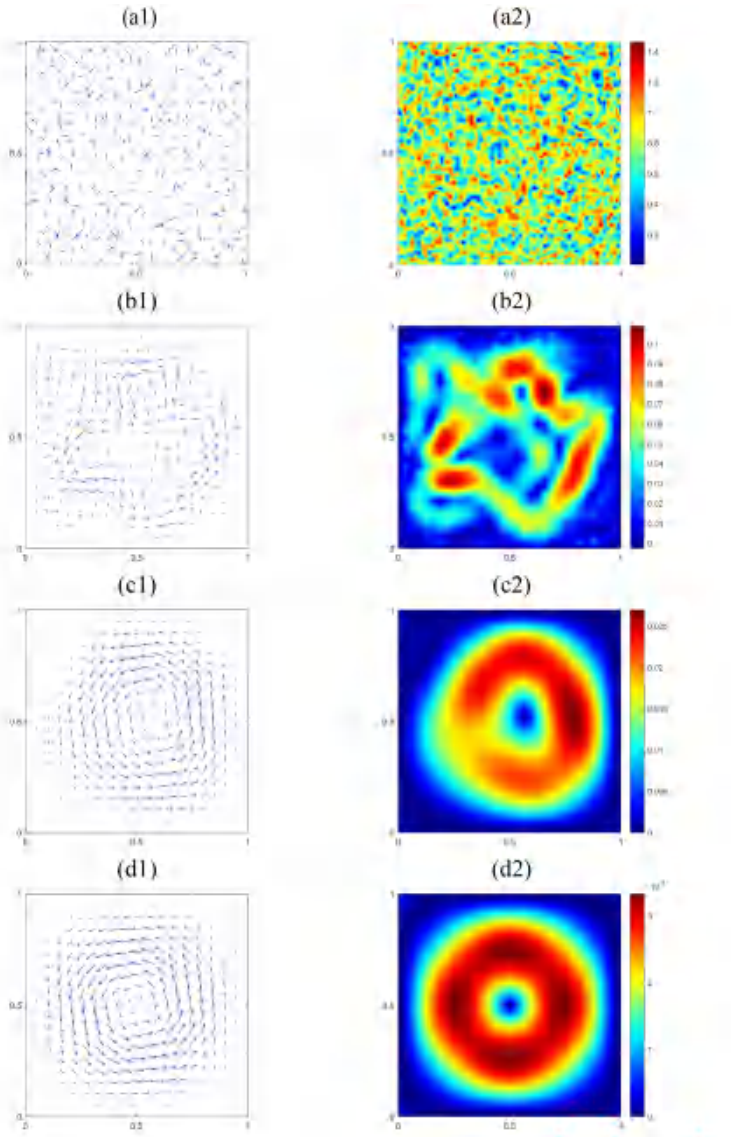

FIGURE 5. Snapshots of the velocity $\boldsymbol{u}$ is taken at (a) $t = 0.00$, (b) $t = 0.01$, (c) $t = 0.10$, (d) $t = 1.00$. For each subfigure, the left is direction of velocity and the right is magnitude of velocity.

In Figure 8, we display the self-organizing of active fluid at different times when the external body force $\boldsymbol{f}(\boldsymbol{x}, t) = (0, 0, 0)$. Due to the active fluid will form a stable vortex with time under different random initial conditions, we choose the movement time of $\boldsymbol{u}$ in Figure 8 is the same as that in Figure 5. According to Figure 8(d1), it can be seen that the stable vortex formed by the active fluid is almost parallel to the xz plane. Therefore, the cross section parallel to the xz plane is used to show the change of velocity magnitude. Different from Figure 5(d2), the velocity magnitude of the active fluid in Figure 8(d2) is asymmetrical in space. In 3D space, the active fluid can move spontaneously along the x, y, and z axes, so the collective direction of motion is not completely parallel to a plane.

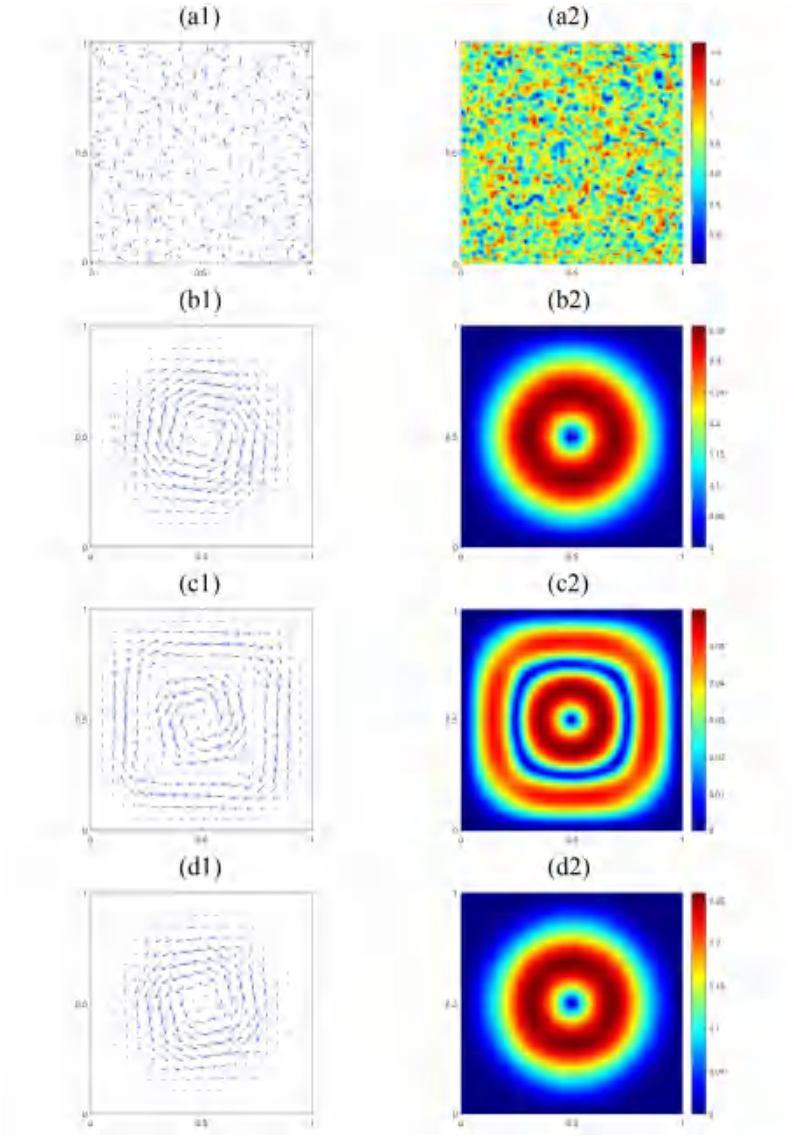

FIGURE 6. Snapshots of the velocity $\boldsymbol{u}$ is taken at (a) $t = 0.00$, (b) $t = 0.50$, (c) $t = 0.72$, (d) $t = 1.00$. For each subfigure, the left is direction of velocity and the right is magnitude of velocity.

Secondly, the external body force is set as follows

$$\boldsymbol{f}(\boldsymbol{x},t) = \begin{cases} (-(\cos(2\pi x+\pi)+1)\times\sin(2\pi y), (\cos(2\pi y+\pi)+1), 0)\times\sin(2\pi x), \\ \quad (x,y,z)\in\left(\frac{1}{4},\frac{3}{4}\right)\times\left(\frac{1}{4},\frac{3}{4}\right)\times(0,1),\ t\in\left[k,k+\frac{1}{2}\right), k=0,1,2,\cdots, \\ ((\cos(2\pi x+\pi)+1)\times\sin(2\pi y), -(\cos(2\pi y+\pi)+1)\times\sin(2\pi x), 0), \\ \quad (x,y,z)\in\left(\frac{1}{4},\frac{3}{4}\right)\times\left(\frac{1}{4},\frac{3}{4}\right)\times(0,1),\ t\in\left[k+\frac{1}{2},k+1\right), k=0,1,2,\cdots. \end{cases}$$

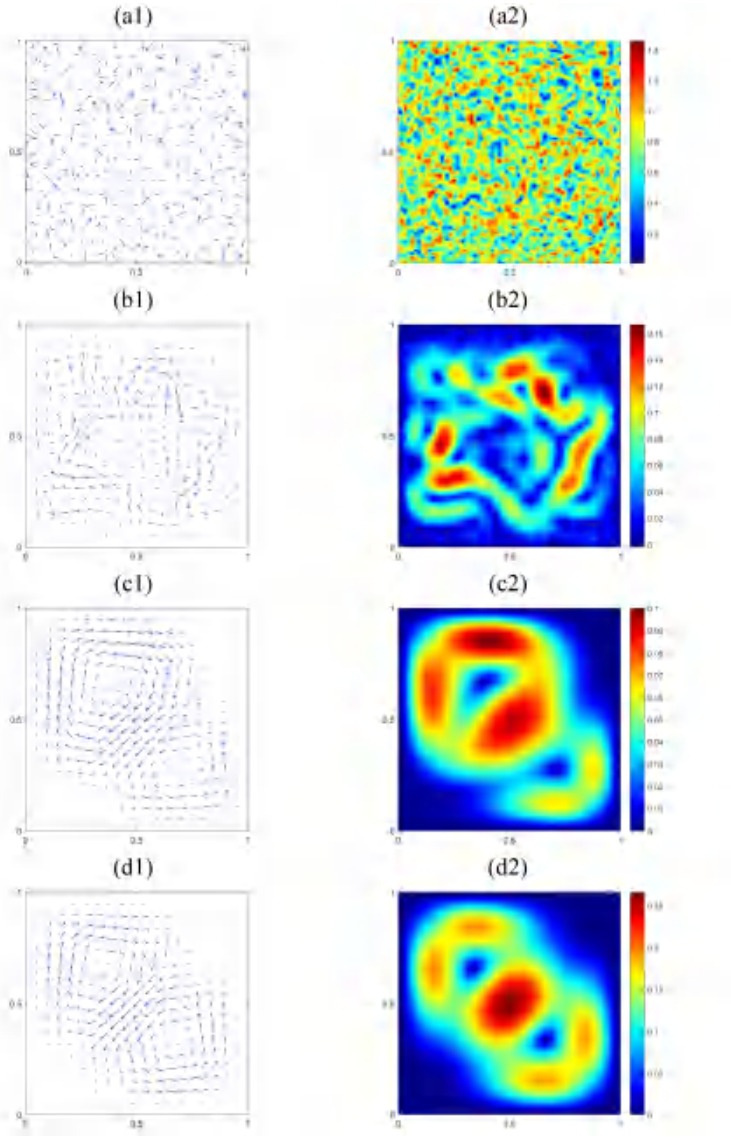

FIGURE 7. Snapshots of the velocity $\boldsymbol{u}$ is taken at (a) $t = 0.00$, (b) $t = 0.01$, (c) $t = 0.10$, (d) $t = 1.00$. For each subfigure, the left is direction of velocity and the right is magnitude of velocity.

The expressions for f_1 and f_2 in 3D are the same as the second simulation in 2D, and let f_3 be equal to 0. The snapshots of $\boldsymbol{u}$ at $t = 0.00$, 0.50, 0.72 and 1.00 are shown in Figure 9. Due to $f_3 = 0$, the magnitude of u_3 tends to 0 in the process of spontaneous aggregation of active fluid to form collective motion, and the stable vortex formed is basically parallel to the xy plane. Therefore, the cross section parallel to the xy plane is selected to show the magnitude change of velocity. It can be seen from Figure 9 and Figure 6 that the numerical simulation results are consistent.

Thirdly, we set the external body force $\boldsymbol{f}(\boldsymbol{x}, t) = (\cos(2\pi y), \cos(2\pi x), 0)$. As shown in Figure 10, the snapshots of $\boldsymbol{u}$ are taken at $t = 0.00$, 0.01, 0.10 and 1.00.

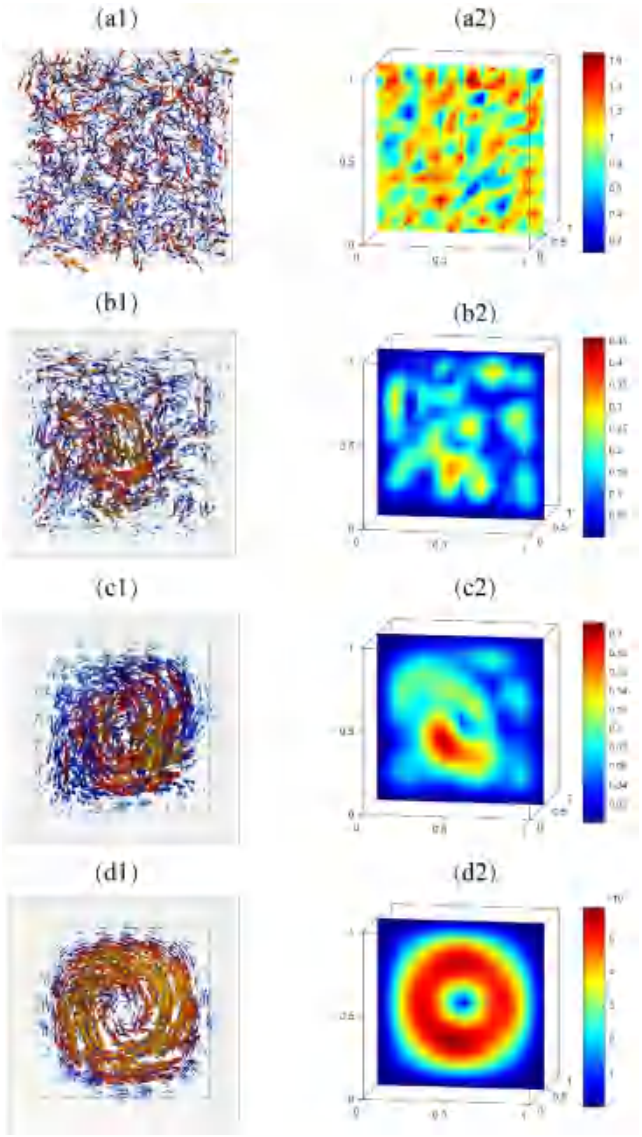

FIGURE 8. Snapshots of the velocity $\boldsymbol{u}$ is taken at (a) $t = 0.00$, (b) $t = 0.01$, (c) $t = 0.10$, (d) $t = 1.00$. For each subfigure, the left is direction of velocity and the right is magnitude of velocity.

We can observe that the active fluid forms two stable vortices from a disordered state. In Figure 10(d1), it is clear that the vortex in the upper left corner moves counterclockwise and the vortex in the lower right corner moves clockwise, which is the opposite of the direction in Figure 7(d1). Due to different initial random values, the active fluid self-organizes into vortex with different collective motion direction. As shown in Figure 9, the stable vortex formed is basically parallel to the xy plane.

6. Concluding remarks

This paper proposes a linear, decoupled and unconditional stable fully discrete mixed finite element numerical scheme for the active fluid model. On the one

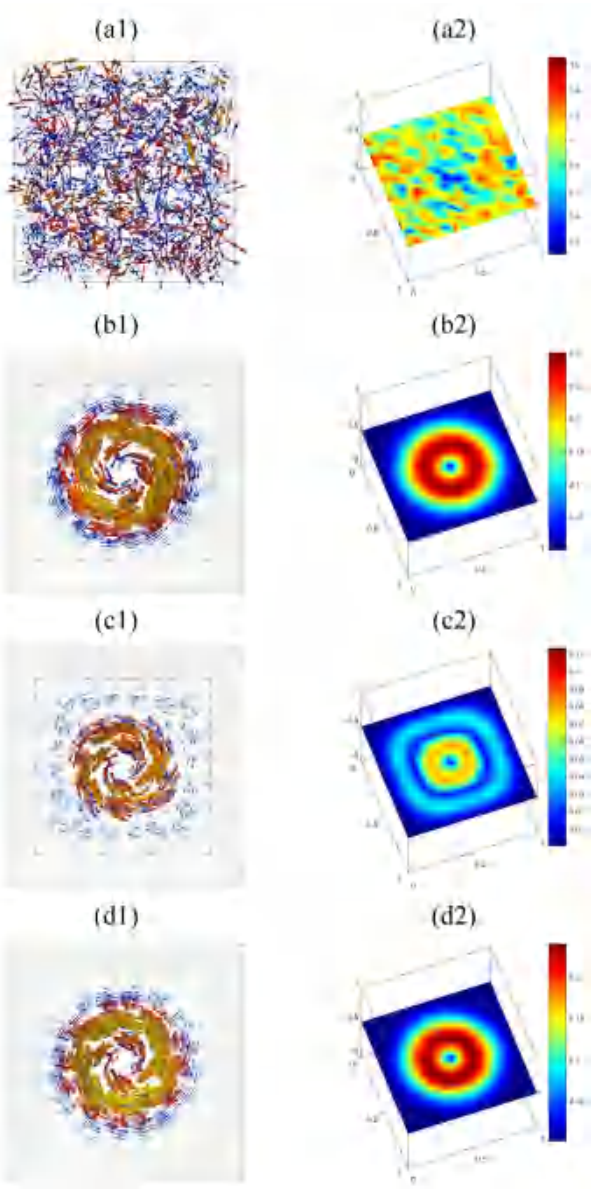

FIGURE 9. Snapshots of the velocity $\boldsymbol{u}$ is taken at (a) $t = 0.00$, (b) $t = 0.50$, (c) $t = 0.72$, (d) $t = 1.00$. For each subfigure, the left is direction of velocity and the right is magnitude of velocity.

hand, the designed scheme can greatly reduce the expensive time cost caused by the fourth-order derivative term, strong nonlinear terms and the coupling of velocity and pressure in numerical calculation. On the other hand, the rigorous and detailed proof processes of solvability and stability are given, and the optimal error estimates of the related variables are obtained through strict theoretical analysis. Furthermore, through ample numerical experiments, the validity of the model and numerical scheme are demonstrated numerically.

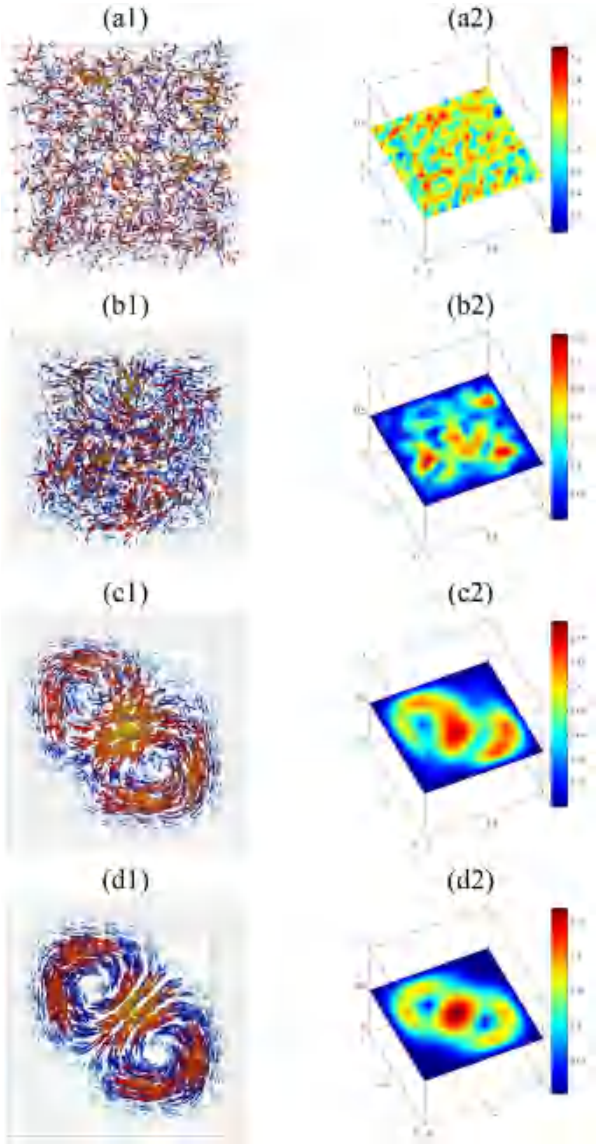

FIGURE 10. Snapshots of the velocity $\boldsymbol{u}$ is taken at (a) $t = 0.00$, (b) $t = 0.01$, (c) $t = 0.10$, (d) $t = 1.00$. For each subfigure, the left is direction of velocity and the right is magnitude of velocity.

Acknowledgments

The authors are grateful to the reviewers for the constructive comments and valuable suggestions which have improved the paper. Bo Wang is supported by the National Natural Science Foundation of China (42430702) and the Natural Science Foundation of Henan Province (232300420109).

Data availability statement

No data was used for the research described in the article.

References

[1] P. Ciarlet, Introduction to linear shell theory(Series in applied mathematics). Elsevier Masson, 1998.

[2] P. Ciarlet, The finite element method for elliptic problems. SIAM, 2002.

[3] A. Cavagna, A. Cimarelli, I. Giardina, et al., Scale-free correlations in starling flocks. Proc. Natl Acad. Sci. USA 107(26), 11865-11870, 2010.

[4] X. Cai, Q. Jiu, Weak and strong solutions for the incompressible Navier-Stokes equations with damping. J. Math. Anal. Appl. 343, 799-809, 2008.

[5] C. Chen, K. Pan, X. Yang, Numerical approximations of a hydro-dynamically coupled phase-field model for binary mixture of passive/active nematic liquid crystals and viscous fluids. Appl. Numer. Math. 158, 1-21, 2020.

[6] Q. Du, M. Gunzburger, Finite-element approximations of a Ladyzhenskaya model for stationary incompressible viscous flow. SIAM J. Numer. Anal. 27(1), 1-19, 1990.

[7] J. Dunkel, S. Heidenreich, K. Drescher, et al., Fluid dynamics of bacterial turbulence. Phys. Rev. Lett. 110(22), 228102, 2013.

[8] J. Dunkel, S. Heidenreich, M. Bär, et al., Minimal continuum theories of structure formation in dense active fluids. New J. Phys. 15(4), 045016, 2013.

[9] X. Dong, Y. He, Two-level newton iterative method for the 2D/3D stationary incompressible magnetohydrodynamics. J. Sci. Comput. 63(2), 426-451, 2015.

[10] J. Elgeti, R. Winkler, G. Gompper, Physics of microswimmers-single particle motion and collective behavior: a review. Rep. Prog. Phys. 78(5), 056601, 2015.

[11] V. Girault, P. Raviart, Finite Element Method for Navier-Stokes equations: theory and Algorithms. Springer, Berlin, 1987.

[12] J. Guermond, P. Minev, J. Shen, An overview of projection methods for incompressible flows. Comput. Methods Appl. Mech. Engrg. 195, 6011-6045, 2006.

[13] F. Hecht, New development in FreeFem++. J. Numer. Math. 20(3-4), 251-265, 2012.

[14] M. Huang, W. Hu, S. Yang, et al., Circular swimming motility and disordered hyperuniform state in an algae system. Proc. Natl. Acad. Sci. USA 118(18), e2100493118, 2021.

[15] E. Jacob, I. Becker, Y. Shapira, et al., Bacterial linguistic communication and social intelligence. TRENDS in Microbiology 12(8), 366-372, 2004.

[16] M. James, W. Bos, M. Wilczek, Turbulence and turbulent pattern formation in a minimal model for active fluids. Phys. Rev. Fluids 3(6), 061101, 2018.

[17] Y. Katz, K. Tunstrøm, C. Ioannou, et al., Inferring the structure and dynamics of interactions in schooling fish. Proc. Natl Acad. Sci. USA 108(46), 18720-18725, 2011.

[18] H. López, J. Gachelin, C. Douarche, et al., Turning bacteria suspensions into superfluids. Phys. Rev. Lett. 115(2), 028301, 2015.

[19] Q. Li, L. Mei, X. Yang, et al., Efficient numerical schemes with unconditional energy stabilities for the modified phase field crystal equation. Adv. Comput. Math. 45, 1551-1580, 2019.

[20] M. Li, D. Shi, Z. Li, et al., Two-level mixed finite element methods for the Navier-Stokes equations with damping. J. Math. Anal. Appl. 470(1), 292-307, 2019.

[21] S. Liu, S. Shankar, M. Marchetti, et al., Viscoelastic control of spatiotemporal order in bacterial active matter. Nature 590(7844), 80-84, 2021.

[22] D. Marenduzzo, E. Orlandini, M. Cates, et al., Steady-state hydrodynamic instabilities of active liquid crystals: hybrid lattice boltzmann simulations. Phys. Rev. E 76(3), 31921, 2007.

[23] F. Nédélec, T. Surrey, A. Maggs, et al., Self-organization of microtubules and motors. Nature 389(6648), 305-308, 1997.

[24] M. Olshanskii, Two-level method and some a priori estimates in unsteady Navier-Stokes calculations. J. Comput. Appl. Math. 104(2), 173-191, 1999.

[25] G. Popkin. The physics of life. Nature 529(7584), 16-18, 2016.

[26] L. Qi, Y. Hou, A second order energy stable BDF numerical scheme for the Swift-Hohenberg equation. J. Sci. Comput. 88(3), 74, 2021.

[27] H. Qiu, L. Mei, Two-grid MFEAs for the incompressible Stokes type variational inequality with damping. Comput. Math. Appl. 78(8), 2772-2788, 2019.

[28] I. Riedel, K. Kruse, J. Howard, A self-organized vortex array of hydrodynamically entrained sperm cells. Science 309(5732), 300-303, 2005.

[29] H. Reinken, D. Nishiguchi, S. Heidenreich, et al., Organizing bacterial vortex lattices by periodic obstacle arrays. Commun. Phys. 3(1), 76, 2020.

[30] J. Ren, B. Wang, G. Zou, A Crank-Nicolson discontinuous Galerkin pressure-projection method for the hydrodynamic and sediment transport model. Comput. Math. Appl. 142, 175-197, 2023.

[31] D. Saintillan, Rheology of Active Fluids. Annu. Rev. Fluid Mech. 50, 563-592, 2018.
[32] J. Shen, On error estimates of the penalty method for unsteady Navier-Stokes equations. SIAM J. Numer. Anal. 32(2), 386-403, 1995.
[33] J. Shen, On error estimates of the projection methods for the Navier-Stokes equations: second-order schemes. Math. Comp. 65, 1039-1065, 1996.
[34] A. Sokolov, I. Aranson, Physical properties of collective motion in suspensions of bacteria. Phys. Rev. Lett. 109(24), 248109, 2012.
[35] G. Sarfati, A. Maitra, R. Voituriez, et al., Crosslinking and depletion determine spatial instabilities in cytoskeletal active matter. Soft Matter 18(19), 3793-3800, 2022.
[36] T. Surrey, F. Nédélec, S. Leibler, et al., Physical properties determining self-organization of motors and microtubules. Science 292(5519), 1167-1171, 2001.
[37] R. Simha, S. Ramaswamy, Hydrodynamic fluctuations and instabilities in ordered suspensions of self-propelled particles. Phys. Rev. Lett. 89(5), 058101, 2002.
[38] V. Schaller, C. Weber, C. Semmrich, et al., Polar patterns of driven filaments. Nature 467(7311), 73-77, 2010.
[39] X. Trepat, E. Sahai, Mesoscale physical principles of collective cell organization. Nat. Phys. 14(7), 671-682, 2018.
[40] J. Toner, Y. Tu, Long-range order in a two-dimensional dynamical XY model: how birds fly together. Phys. Rev. Lett. 75(23), 4326-4329, 1995.
[41] J. Toner, Y. Tu, S. Ramaswamy, Hydrodynamics and phases of flocks. Annals of Physics 318(1), 170-244, 2005.
[42] D. Volfson, S. Cookson, J. Hasty, et al., Biomechanical ordering of dense cell populations. Proc. Natl Acad. Sci. USA 105(40), 15346-15351, 2008.
[43] C. Wolgemuth, Collective swimming and the dynamics of bacterial turbulence. Biophysical Journal 95(4), 1564-1574, 2008.
[44] H. Wensink, J. Dunkel, S. Heidenreich, et al., Meso-scale turbulence in living fluids. Proc. Natl. Acad. Sci. USA 109(36), 14308-14313, 2012.
[45] H. Wioland, E. Lushi, R. Goldstein, Directed collective motion of bacteria under channel confinement. New J. Phys. 18(7), 075002, 2016.
[46] J. Wu, A. Roman, J. Carvajal-Gonzalez, et al., Wg and Wnt4 provide long-range directional input to planar cell polarity orientation in Drosophila. Nature Cell Biol. 15(9), 1045-1055, 2013.
[47] X. Wang, G. Zou, B. Wang, The stabilized penalty-projection finite element method for the Navier-Stokes-Cahn-Hilliard-Oono system. Appl. Numer. Math. 165, 376-413, 2021.
[48] C. Wang, J. Wang, Z. Xia, et al., Optimal error estimates of a Crank-Nicolson finite element projection method for magnetohydrodynamic equations. ESAIM Math. Model. Numer. Anal. 56(3), 767-789, 2022.
[49] C. Xu, C. Chen, X. Yang, Efficient, non-iterative, and decoupled numerical scheme for a new modified binary phase-field surfactant system. Numer. Algorithms 86, 863-885, 2021.
[50] X. Yang, Numerical approximations of the Navier-Stokes equation coupled with volume-conserved multi-phase-field vesicles system: fully-decoupled, linear, unconditionally energy stable and second-order time-accurate numerical scheme. Comput. Methods Appl. Mech. Engrg. 375, 113600, 2021.
[51] X. Yang, G. Zhang, X. He, Convergence analysis of an unconditionally energy stable projection scheme for magneto-hydrodynamic equations. Appl. Numer. Math. 36, 235-256, 2019.
[52] X. Yang, Z. Cui, M. Forest, et al., Dimensional robustness and instability of sheared, semidilute, nanorod dispersions. Multiscale Model Sim. 7(2), 622-654, 2008.
[53] H. Zhang, A. Béer, E. Florin, et al., Collective motion and density fluctuations in bacterial colonies. Proc. Natl. Acad. Sci. USA 107(31), 13626-13630, 2010.
[54] J. Zhang, C. Chen, X. Yang, A novel decoupled and stable scheme for an anisotropic phase-field dendritic crystal growth model. Appl. Math. Lett. 95, 122-129, 2019.
[55] J. Zhang, C. Chen, X. Yang, et al., Efficient numerical scheme for a penalized Allen-Cahn type Ohta-Kawasaki phase-field model for diblock copolymers. J. Comput. Appl. Math. 378, 112905, 2020.
[56] G. Zhang, X. He, X. Yang, A decoupled, linear and unconditionally energy stable scheme with finite element discretizations for magneto-hydrodynamic equations. J. Sci. Comput. 81(3), 1678-1711, 2019.
[57] J. Zhang, X. Yang, Numerical approximations for a new L^2-gradient flow based phase field crystal model with precise nonlocal mass conservation. Comput. Phys. Commun. 243, 51-67, 2019.

[58] G. Zou, Z. Li, X. Yang, Fully discrete discontinuous Galerkin numerical scheme with second-order temporal accuracy for the hydrodynamically coupled lipid vesicle model. J. Sci. Comput. 95(5), 1-47, 2023.
[59] G. Zou, B. Wang, X. Yang, A fully-decoupled discontinuous Galerkin approximation of the Cahn-Hilliard-Brinkman-Ohta-Kawasaki tumor growth model. ESAIM-math. Model. Num. 56(6), 2141-2180, 2022.

School of Mathematics and Statistics, Henan University, Kaifeng 475004, P. R. China
E-mail: yuxingzhang@henu.edu.cn

School of Mathematics and Statistics, Henan University, Kaifeng 475004, P. R. China, Henan Key Laboratory of Earth System Observation and Modeling, Henan University, Kaifeng 475004, P. R. China, The Academy for Advanced Interdisplinary Studies, Henan University, Zhengzhou 450046, P. R. China
E-mail: wb2008@henu.edu.cn